Open Access

IJCER ONLINE

ISSN Online: 2250–3005

Impact Factor: 1.145

IJCER - International Journal of Computational Engineering Research

Volume 05 - Issue 07 , (July 2015)

www.ijceronline.com– Email–ijceronline@gmail.com

Editorial Board

Editor-In-Chief

Editorial Committees

Contents:

ISSN (e): 2250 – 3005 || Volume, 05 || Issue, 07 || July – 2015 ||
International Journal of Computational Engineering Research (IJCER)

Some Oscillation Properties of Third Order Linear Neutral Delay Difference Equations

A.George Maria Selvam[1], M. Paul Loganathan[2], K.R.Rajkumar[3]
[1,3] *Sacred Heart College, Tirupattur – 635 601, S.India,*
[2] *Dravidian University, Kuppam*

ABSTRACT
In this paper, we establish ***some sufficient*** *conditions for the oscillation of solutions of third order linear neutral delay difference equations of the form*
$\Delta\left(a(n)\Delta^2(x(n)+p(n)x(\tau(n)))\right)+q(n)x(\sigma(n))=0.$

I. INTRODUCTION

In this paper, we consider the third order linear neutral delay difference equations from

$$\Delta\left(a(n)\right)\Delta^2\left(x(n)+p(n)x(\tau(n)))\right)+q(n)x(\sigma(n))=0 \qquad (1)$$

where $n\in N(n_0)=\{n_0,n_0+1..,\}$, n_0 is a nonnegative integer, subject to the following conditions

(H_1) $a(n), p(n), q(n)$ are positive sequences.

$0\le p(n)\le p\le 1, \tau(n)\le n, \sigma(n)\le n, \lim_{n\to 0}\tau(n)=\lim_{n\to 0}\sigma(n)=\infty$ and $R(n)=\sum_{s=n_0}^{n-1}\frac{1}{a(s)}\to\infty$ as $n\to\infty$

$$(H_2)\sum_{n=n_0}^{\infty}\sum_{s=n_0}^{\infty}\left(\frac{1}{a(s)}\sum_{t=n}^{\infty}q(t)\right)=\infty.$$

$$(H_3)\limsup_{n\to\infty}\sum_{s=n_0}^{n-1}q(s)(1-p(\sigma(s)))\left(\frac{KM(\sigma(s))^2}{2}\right)-\frac{a^2(s+1)}{4sa(s)}=\infty.$$

We set $z(n)=x(n)+p(n)x(\tau(n))$.

The oscillation theory of difference equations and their applications have received more attention in the last few decades, see [[1]-[4]], and the references cited therein. Especially the study of oscillatory behavior of second order equations of various types occupied a great deal of interest. However the study of third order difference equations have received considerably less attention even though such equations have wide applications. In [[5]-[10]] the authors investigated the oscillatory properties of solutions of third order delay difference equations and in [[11]-[15]]. Motivated by the above observations, in this paper, we investigate the oscillatory behavior of solutions of equation (1).

Let $\theta=\max\left\{\lim_{\delta x\to 0}\sigma(n),\tau(n)\right\}$. By a solution of equation (1) we mean a real sequence *x(n)* which is defined for all $n\ge n_0-\theta$ satisfying (1) for all $n\ge n_0$. A non-trivial solution *x(n)* is said to be oscillatory if it is neither eventually positive or eventually negative; otherwise, it is nonoscillatory. Equation (1) is said to be oscillatory if all its solutions are oscillatory.

II. MAIN RESULTS

Lemma 2.1. Let *x(n)* be a positive solution of equation (1) for all $n\ge n_0$ such $x(n)>0, \Delta x(n)\ge 0,$ and $\Delta^2 x(n)\le 0$ on $[n_1,\infty)$ for some $n_1\ge n_0$. Then for each k with 0 < k < 1, there exists $n_2\ge n_1$ such that

$$\frac{x(n-\sigma)}{x(n)}\ge k\frac{n-\sigma}{n}, n\ge n_2. \qquad (2)$$

Proof. From the Lagrange's Mean value theorem, we have for $n\ge n_1$, for some k

$$\Delta x(k) = \frac{x(n) - x(\sigma(n))}{n - \sigma(n)} \text{ ; for some k} \qquad (3)$$

such that $\sigma(n) < k < n.\Delta^2 x(n) \le 0$ and $\Delta x(n)$ is non-increasing, which implies that $\Delta x(k) < \Delta x(\sigma(n))$ and hence, using equation (3)

$$x(n) \le x(\sigma(n)) + \Delta x(\sigma(n))(n - \sigma(n))$$

$$\frac{x(n)}{x(\sigma(n))} \le 1 + \frac{\Delta x(\sigma(n))}{x(\sigma(n))}(n - \sigma(n)) \qquad (4)$$

Apply Lagrange's Mean value theorem once again for *x(n)* on $[n_1, \sigma(n)]$ for $n \ge n_1 + \sigma(n)$. Now

$\Delta x(c) = \frac{x(\sigma(n)) - x(n_1)}{\sigma(n) - n_1}$ for some c such that $n_1 < c < \sigma(n)$ and $\Delta x(c) > \Delta x(\sigma(n))$ which implies $x(\sigma(n)) \ge \Delta x(\sigma(n))(\sigma(n) - n_1)$. Hence

$$\frac{x(\sigma(n))}{\Delta x(\sigma(n))} \ge \sigma(n) - n_1$$

For $K \in (0,1)$, we can find $n_2 \ge n_1 + \sigma$

$$\frac{x(\sigma(n))}{\Delta x(\sigma(n))} \ge K\sigma(n) \text{ for } n \ge n_2 \qquad (5)$$

From equation (4) and for all $n \ge n_2$, we have

$$\frac{x(n)}{x(\sigma(n))} \le 1 + \frac{1}{K\sigma(n)}(n - \sigma(n))$$

$$\le 1 + \frac{n}{K\sigma(n)} - \frac{\sigma(n)}{K\sigma(n)}$$

$$\le \frac{n}{K(\sigma(n))}$$

Hence,

$$\frac{x(\sigma(n))}{x(n)} \ge \frac{K(\sigma(n))}{n} \qquad (6)$$

Lemma 2.2 Let *x(n)* be a positive solution of equation (1), then the corresponding sequence *z(n)* satisfies the following condition *z(n)* > 0, $\Delta z(n) > 0$, $\Delta^2 z(n) > 0$, $\Delta^3 z(n) > 0$ for some $n_1 \ge n_0$. Then there exits $n_2 \ge n_1$ such that $\frac{z(n)}{\Delta z(n)} \ge \frac{Mn}{2}$, $n \ge n_2$ for each M, 0 < M < 1.

Proof. We define a function H(n) for $n \ge n_2 \ge n_1$, as

$$H(n) = (n - n_2)z(n) - \frac{M(n - n_2)^2}{2}\Delta z(n) \qquad (7)$$

$$\Delta H(n) \ge z(n) + (n - n_2)\Delta z(n) - \frac{M(n - n_2)^2}{2}\Delta^2 z(n) \qquad (8)$$

By Taylor's Theorem,

$$z(n) \ge z(n_2) + (n - n_2)\Delta z(n_2) + \frac{(n - n_2)^2}{2}\Delta^2 z(n)$$

From (8)

$$\Delta H(n) \ge z(n_2) + (n - n_2)\Delta z(n_2) + \frac{(n - n_2)^2}{2}\Delta^2 z(n) + (n - n_2)\Delta z(n) - \frac{M(n - n_2)^2}{2}\Delta^2 z(n)$$

which implies $\Delta H(n) > 0$ and $H(n+1) > H(n) > H(n_2) = 0$ for every $n \ge n_2$ from (7)

$$(n-n_2)z(n)-\frac{M(n-n_2)^2}{2}\Delta z(n)>0$$

which implies $\frac{z(n)}{\Delta z(n)}\geq\frac{Mn}{2}$ for $n\geq n_2$.

Theorem 2.3. Assume that (H_1) to (H_2) hold, then equation (1) is oscillatory.

Proof: Suppose, if possible that the equation (1) has a nonoscillatory solution. Without loss of generality suppose that x(n) is a positive solution of equation (1). We shall discuss the following cases for *z(n).*

(i) $z(n)>0,\ \Delta z(n)<0,\ \Delta^2 z(n)>0,\ \Delta^3 z(n)\leq 0,$

(ii) $z(n)>0,\ \Delta z(n)>0,\ \Delta^2 z(n)>0,\ \Delta^3 z(n)\leq 0,$

Case 1. $z(n)>0,\ \Delta z(n)<0,\ \Delta^2 z(n)>0,\ \Delta^3 z(n)\leq 0,$

Since z(n) > 0and $\Delta z(n)<0,$ then there exists finite limits $\lim_{n\to\infty} z(n)=k$. We shall prove that k = 0.

Assume that k > 0. Then for any $\in>0$, we have $k+\in> z(n)>k$. Let $0<\in<\frac{k(1-p)}{p}$, we have $k+\in> x(n)>k-p(n)x(\tau(n))$.

$$x(n)>k-p(k+\in)=m(k+\in)$$
$$x(n)>mz(n)$$

When $m=\frac{k-p(k+\in)}{(k+\in)}$. Now from the equation (1) we have

$$\Delta\left(a(n)\Delta^2\left(\left(x(n)+p(n)x(\tau(n))\right)\right)\right)=-q(n)x(\sigma(n))-\Delta\left(a(n)\Delta^2 z(n)\right)\geq q(n)mz(\sigma(s))$$

Summing the above inequality from n to ∞ we get,

$$-\sum_{t=n}^{\infty}\Delta\left(a(t)\Delta^2 z(t)\right)\geq m\sum_{s=n}^{\infty}q(s)z(\sigma(s))$$
$$a(n)\Delta^2 z(n)\geq m\sum_{s=n}^{\infty}q(s)z(\sigma(s))$$

Using the fact that $z(\sigma(n))\geq k$ we obtain, $a(n)\Delta^2 z(n)\geq mk\sum_{s=n}^{\infty}q(s)$ which implies

$\Delta^2(z(n))\geq mk\left(\frac{1}{a(n)}\sum_{s=n}^{\infty}q(s)\right)$. Summing from n to ∞ we have,

$$\sum_{s=n}^{\infty}\Delta^2 z(s)\geq mk\sum_{s=n}^{\infty}\left(\frac{1}{a(s)}\sum_{t=s}^{\infty}q(t)\right)$$
$$-\Delta z(n)\geq mk\sum_{s=n}^{\infty}\left(\frac{1}{a(s)}\sum_{t=s}^{\infty}q(t)\right)$$

Summing the last inequality n_1 to ∞

$$z(n_1)\geq mk\sum_{n=n_1}^{\infty}\sum_{s=n}^{\infty}\left(\frac{1}{a(s)}\sum_{t=s}^{\infty}q(t)\right)$$

This contradicts (H_2). Thus k = 0. Moreover, the inequality, $0\leq x(n)\leq z(n)$ implies $\lim_{n\to\infty}x(n)=0$.

Case 2. $z(n)>0,\ \Delta z(n)>0,\ \Delta^2 z(n)>0,\ \Delta^3 z(n)\leq 0,$

We have x(n) = z(n) - p(n) $x(\tau(n))$, we obtain further

$$x(\sigma(n))=z(\sigma(n))-p(\sigma(n))x(\sigma(n)-\tau)$$
$$\geq z(\sigma(n))-p(\sigma(n))x(\sigma(n))$$

$$\geq (1-p(\sigma(n)))z(\sigma(n)).$$

From equation (1) we have,

$$\Delta\left(a(n)\Delta^2 z(n)\right) \leq -q(n)x(\sigma(n))$$

$$\Delta\left(a(n)\Delta^2 z(n)\right) \leq -q(n)(1-p(\sigma(n)))z(\sigma(n))$$

$$w(n) = n\frac{a(n)\Delta^2 z(n)}{\Delta z(n)}, n \geq n_1 \tag{9}$$

$$\Delta w(n) = \left(\frac{a(n+1)\Delta^2 z(n+1)}{\Delta z(n+1)}\right) + n\left(\Delta\left(\frac{a(n)\Delta^2 z(n)}{\Delta z(n)}\right)\right)$$

$$= \frac{w(n+1)}{n+1} + n\left(\frac{\Delta(a(n)\Delta^2 z(n))}{\Delta z(n+1)} - \frac{a(n)\Delta^2 z(n)\Delta^2 z(n)}{\Delta z(n)\Delta z(n+1)}\right)$$

$$\leq \frac{w(n+1)}{n+1} + n\left(\frac{\Delta(a(n)\Delta^2 z(n))}{\Delta z(n)} - a(n)\frac{(\Delta^2 z(n+1))^2}{(\Delta z(n+1))^2}\right)$$

$$\leq \frac{w(n+1)}{n+1} - \frac{nq(n)(1-p(\sigma(n)))z(\sigma(n))}{\Delta z(n)} - \frac{na(n)}{(n+1)^2 a^2(n+1)}w^2(n+1) \tag{10}$$

Also from Lemma (2.1) with x(n) = $\Delta z(n)$

$$\frac{x(\sigma(n))}{x(n)} \geq \frac{K\sigma(n)}{n}, \sigma(n) \geq n$$

$$\frac{\Delta z(\sigma(n))}{\Delta z(n)} \geq \frac{K\sigma(n)}{n} \tag{11}$$

$$\frac{1}{\Delta z(n)} \geq \frac{K\sigma(n)}{n}\frac{1}{\Delta z(\sigma(n))} \text{ for } \sigma(n) \geq n_1 \geq n_2.$$

By Lemma (2.2)

$$\frac{z(\sigma(n))}{\Delta z(n)} \geq \frac{K\sigma(n)}{n}\frac{z(\sigma(n))}{\Delta z(\sigma(n))}$$

$$\geq \frac{K\sigma(n)}{n}\frac{M\sigma(n)}{2} \tag{12}$$

$$\frac{z(\sigma(n))}{\Delta z(n)} \geq \frac{KM}{2}\frac{(\sigma(n))^2}{n}$$

Using (11) and (12) in (10)

$$\Delta w(n) \leq -q(n)(1-p(\sigma(n)))\left(\frac{KM\sigma^2(n)}{2}\right) + \frac{w(n+1)}{n+1} - \frac{na(n)}{(n+1)^2 a^2(n+1)}w^2(n+1) \tag{13}$$

Using the inequality

$$Vx - Ux^2 \leq \frac{1}{4}\frac{V^2}{U}, U > 0$$

And put $x = w(n+1), V = \frac{1}{n+1}, U = \frac{na(n)}{(n+1)^2 a^2(n+1)}$, we have

$$\frac{w(n+1)}{(n+1)} - \frac{na(n)}{(n+1)^2 a^2(n+1)}w^2(n+1) \leq \frac{a^2(n+1)}{4na(n)} \tag{14}$$

From equation (13)

$$\Delta w(n) \le -nq(n)(1-p(\sigma(n)))\left(\frac{KM}{2}\frac{(\sigma(n))^2}{n}\right)+\frac{a^2(n+1)}{4na(n)} \qquad (15)$$

Summing the last inequality from n_2 to $n-1$ we obtain

$$\sum_{n=n_2}^{n-1} q(s)(1-p(\sigma(s)))\left(\frac{KM(\sigma(s))^2}{2}\right)-\frac{a^2(s+1)}{4sa(s)} \le w(n_2)$$

Taking lim sup in the above inequality, we obtain contradiction with H_3.

REFERENCES

[1] R. P. Agarwal, Difference and Equations and Inequalities, 2nd Edition, Marcel Dekker, New York, 2000.
[2] R. P. Agarwal, M. Bohner, S. R. Grace and D. O. Regan, Discrete Oscillation Theory, Hindawi, New York, 2005.
[3] R. P. Agarwal, S. R. Grace and D. O. Regan, Oscillation Theory for Difference and Funtional Differential Equations, Kluwer, Dordrecht, 2000.
[4] S. H. Saker, Oscillation theory of delay differential and difference equations second and third orders, Lambert Academic Publishing (2010).
[5] R. P Agarwal, M. F. Aktas, A. Tiryaki, On oscillation criteria for third order nonlinear delay differential equations, Arch. Math (Brno), 45 (2009), 1 - 18.
[6] S. R. Grace, R. P Agarwal, R. Pavani, E. Thandapani, On the oscillation of criteria third order nonlinear functional differential equations, Appl.Math.Comp.,202(2008),102-112.
[7] S .H. Saker, Oscillation criteria of third order nonlinear delay differential equations, Mathematics Solvaca, Vol.56, no.4 (2006) pp. 433 - 450.
[8] J. Dzurina, E. Thandapani and S. Tamilvanan, Oscillatory solutions to third order half-linear netural differential equations, Elec. J.diff. Eqns., Vol 2012 (2012), No.29, pp. 1 - 9.
[9] B. Baculikova and J. Dzurina, Oscillation of third order netural differential equations, Math. Comp. Modelling, 52(2010), 215 – 226.
[10] On the Oscillation of Third Order Linear Neutral delay Differential Equations, K V V seshagiri rao, P. V H S Sai Kumar I JMTT Vol4, Issue 11 December 2013.
[11] R. P. Agarwal, S. R. Grace and D. O. Regan, On the oscillation of certain third order difference equations, Adv. Differ. Eqn., 3(2005), 345 - 367.
[12] S. R. Grace, R. P. Agarwal and J. R. Graef, Oscillation criteria for certain third order non-linear difference equations, Appl. Anal. Discrete Math., 3(2009), 27 - 38.
[13] J. R. Graef and E. Thandapani, Oscillatory and asymptotic behavior of solutions of third order delay difference equations, Funkcial. Ekvac.42(1999), 355 - 369.
[14] S. H. Saker, Oscillation of third order difference equations, Port. Math., 61(2004), 249-257.
[15] S. H. Saker, Oscillation asymptotic behavior of third order nonlinear neutral delay difference equations, Dyna.Sys.,15(2006)549-568.

ISSN (e): 2250 – 3005 || Volume, 05 || Issue, 07 || July – 2015 ||
International Journal of Computational Engineering Research (IJCER)

Stochastic Model to Find the Characteristic Function of Insulinotropic Action of Glucose-Dependent Insulinotropic Hormone Using Compound Poisson Process

Dr. P. Senthil Kumar * and Ms. R. Abirami**

** Assistant Professor, Department of Mathematics, Rajah Serfoji Government Arts College, Thanjavur, India.*
*** Assistant Professor, Department of Basic Science and Humanities, Ponnaiyah Ramajayam Engineering College, Thanjavur, India.*

ABSTRACT:

The purpose of the Study was to evaluate the comparison of insulinotropic actions of exogenous incretin hormones GIP(Glucose-dependent Insulinotropic Hormone) in Nine type-2 diabetic patients and in Nine age- and weight-matched normal subjects. An oral glucose challenge (75g/300ml) was performed in the morning after an overnight fast between the two distinct groups. The GIP response after oral glucose tended to be lower in the type-2 diabetic patients than normal subjects. In this paper, the problem is investigated by valuation of the characteristic equation obtained by applying Laplace transform to the second order delay differential equation represented by a general version of compound Poisson process.

Key Words: *GIP, Exogenous Incretin hormone, type-2 diabetic, Poisson process, Brownian motion, type-2diabetic patients.****2010 Mathematics Subject Classification:*** *60G50; 60G51; 60G55*

I. INTRODUCTION

In normal subjects, oral glucose enhances insulin secretion more than does intravenous glucose infusion [3], [18], [15], [16]. This augmentation of insulin secretion is due to the secretion and action of gut hormones with insulinotropic activity, namely glucose-dependent insulinotropic hormone; [6], [17] from the upper gut [2]. In type-2 diabetic patients, the incretin effect is reduced or lost [16], [20]. This does not seem to be a consequence of deficient release of GIP, in that most studies found a normal or even enhanced secretion of this incretin hormone in type-2 diabetic patients [11], [4]. By using GIP of the porcine aminoacid sequence, several studies have uniformly described reduced insulinotropic effectiveness in type-2 diabetic patients as compared to normal subjects [9], [12]. Human GIP differs by two amino acids [9], [7] from porcine GIP [10], [14]. GIP responses after oral glucose tended to be lower in the type-2 diabetic patients.

In this paper the problem is investigated by valuation of the characteristic equation obtained by applying Laplace transform to the second order delay differential equation. The jump part in our model is represented by a general version of compound Poisson process. We incorporate a jump part in the stochastic model with delay [1]. We find some analytical closed forms for the expectation of the realized continuously sampled variance. The jump part in our model is represented by a general version of compound Poisson processes, and the expectation and the covariance of the jump sizes are assumed to be deterministic function.

Notations:

β	Scale parameter for model.
λ	Mean rate
$K(t)$	Brownian Motion
$I(t)$	Martingale
$E^*(y)$	Expected value of realized variance
$\Psi(q)$	Characteristic function

II. STOCHASTIC MODEL

2.1. Compound Poisson Process case

Let us consider the jumps represented by a compound Poisson Process, and it seems to allow the jump size to be a random number but not always one in Poisson Process, the model is more realistic.

The stochastic model can be defined as follows:

$$\frac{d\rho^2(t,Q_t)}{dt} = \beta U + \frac{\gamma}{s}\left[\int_{t-s}^{t} \rho(q,Q_q)dK^*(q) + \int_{t-s}^{t} x_q dM(q) - (\lambda - r)s\right]^2 - (\gamma+\beta)\rho^2(t,Q_t) \quad \text{------ (1)}$$

where $K^*(t)$ is a Brownian motion, M(t) is a Poisson Process with intensity μ , and x_t is the jump size at time t which is identically independent normally distributed random variable. We assume that the mean of x_t is σ and the variance of x_t is δ. The Poisson intensity μ and the jump size x_t do not change since they are independent of the Brownian motion.

The Brownian motion and the compound Poisson process are independent. Letting

$y(t) = E^*[\rho^2(t,Q_t)]$,

we obtain the following equation:

$$\frac{dy(t)}{dt} = \beta U + \frac{\gamma}{s}\left[t - \int_{t-s}^{t} y(q)dq + Var^*\left(\sum_{t-s\le q\le t} x_q\right) + \left(E^*\left(\sum_{t-s\le q\le t} x_q\right)\right)^2 + (\lambda-r)^2 s^2 - 2E^*\left(\sum_{t-s\le q\le t} x_q\right)(\lambda-r)s\right] - (\gamma+\beta)y(t)$$

---- (2)

$$= \beta U + \gamma\mu(\sigma^2+\delta) + \gamma\mu^2 s\sigma^2 - 2\gamma\mu s\sigma(\lambda-r) + \gamma s(\lambda-r)^2 + \frac{\gamma}{s}\int_{t-s}^{t} y(q)dq - (\gamma+\beta)y(t)$$

From this equation, if $\sigma = 1$ and $\delta = 0$, , the compound Poisson process is just a Poisson process, and then (2) becomes

$$\frac{dy(t)}{dt} = \beta U + \gamma\mu + \gamma\mu^2 s - 2\gamma\mu s(\lambda-r) + \gamma s(\lambda-r)^2 + \frac{\gamma}{s}\int_{t-s}^{t} y(q)dq - (\gamma+\beta)y(t) \quad \text{------ (3)}$$

Equation (2) has a stationary solution

$$y(t) \equiv Z = U + \frac{\left[\gamma\mu(\sigma^2+\delta) + \gamma\mu^2 s\sigma^2 - 2\gamma\mu s\sigma(\lambda-r) + \gamma s(\lambda-r)^2\right]}{\beta}$$

$$= U + D \ . \quad \text{------- (4)}$$

Where D = $\frac{\gamma}{\beta}\left[\mu(\sigma^2+\delta) + s(\mu\sigma - \lambda + r)^2\right]$

The expectation of the realized variance for compound Poisson jump in stationary regime under risk neutral measure P* is equal to

$$F_{\text{var}} = E^*[y] = \frac{1}{W}\int_0^W y(t)dt = U + D \quad \text{------- (5)}$$

In general case, we substitute $y(t) = Z + Ce^{\tau t}$ in (2) where X is defined in (4).

Then the characteristic equation for τ is

$$\tau = \frac{\gamma}{\tau s}(1 - e^{-\tau s}) - (\gamma+\beta) \quad \text{------ (6)}$$

Therefore, the only solution to this equation is $\tau \approx -\beta$,and by the same method, we have,

$$y(t) = Z + Ce^{-\beta t} = U + D + Ce^{-\beta t}, \qquad \text{------ (7)}$$

$$C = \rho_0^2 - U - D. \qquad \text{------- (8)}$$

Hence, the expectation of the realized variance under risk-neutral measure P* is equal to

$$F_{\text{var}} = E^*[y] = \frac{1}{W}\int_0^W y(t)dt \approx U + D + C\frac{1-e^{-\beta t}}{\beta t}, \qquad \text{------- (9)}$$

Where C is given by (8)

Of course, (9) can also be written as

$$F_{\text{var}} \approx Z + (\rho_0^2 - Z)\frac{1-e^{-\beta t}}{\beta t} \qquad \text{------- (10)}$$

Where Z is given by (4)

Remark: It is interesting to see that when $s = 0$, which means there is no delay in the model, we have that

$$E^*[y] \approx \frac{1-e^{-\beta t}}{\beta t}\left(\rho_0^2 - U - \frac{\gamma\mu(\sigma^2+\delta)}{\beta}\right) + U + \frac{\gamma\mu(\sigma^2+\delta)}{\beta}. \qquad \text{----- (11)}$$

2.2. General Case

In the previous section, we assume that the mean value and variance of the jump size x_t, in the compound Poisson process are constants. Now we consider a more general case in which they are deterministic functions. The approach used in this section is different from the previous ones, which is a more general method and can be applied to derive the same formulae in the previous simple cases.

The stochastic model can be defined by

$$\frac{d\rho^2(t,Q_t)}{dt} = \beta U + \frac{\gamma}{s}\left[\int_{t-s}^{t}\rho(q,Q_q)dK^*(q) + \int_{t-s}^{t}x_q\,dM(q) - (\lambda - r)s\right]^2 - (\gamma+\beta)\rho^2(t,Q_t) \qquad \text{---- (12)}$$

Where K*(t) is a Brownian motion, M*(t)* is a Poisson process with intensity μ, and x_t is the jump size at time t. We assume *that* $E[x_t] = A(t)$, $E[x_q x_t] = C(q,t)$, $q < t$, and $E[x_t^2] = B(t) = C(t,t)$, where A(t), B(t) and C(q, t) are all deterministic functions. Note that the change of measure does not change the Poisson intensity μ and the distribution of jump size x_t, since they are independent of the Brownian motion.

Let $y(t) = E^*[\rho^2(t,Q_t)]$ and take the expectation under risk-neutral probability *P** on both sides of (12). Noting that the Brownian motion and the Poisson process are independent, we obtain the following equation:

$$\frac{dy(t)}{dt} = \beta U + \frac{\gamma}{s}\left[\int_{t-s}^{t}y(q)dq + E^*\left(\int_{t-s}^{t}x_q dM(q)\right)^2 + (\lambda - r)^2 s^2 - 2E^*\left(\int_{t-s}^{t}x_q dM(q)\right)(\lambda - r)s\right] - (\gamma+\beta)y(t).$$

--------- (13)

In order to compute the two expectations in this equation, we first introduce two lemmas as follows [5].

Lemma2.3. Define $I(t) = \int_0^t x_q d(M(q) - \mu q);$ *;* then I(t) is a martingale and EI(t) = 0.

Lemma2.4. Define $I(t) = \int_0^t x_q d(M(q) - \mu q);$ then $EI^2(t) = \mu E\int_0^t x_q^2 dq$.

Therefore,

$$E^*\left(\int_{t-s}^{t}x_q dM(q)\right) = E^*\left(\int_{t-s}^{t}x_q d(M(q) - \mu q)\right) + E^*\left(\int_{t-s}^{t}x_q d\mu q\right)$$

$$= \mu E^*\left(\int_{t-s}^{t} x_q dq\right) \qquad \text{------- (14)}$$

$$= \mu \int_{t-s}^{t} A(q)dq\,,$$

$$E^*\left(\int_{t-s}^{t} x_q dM\ (q)\right)^2 = E^*\left(\int_{t-s}^{t} x_q d\,(M\ (q) - \mu q)\right)^2 + E^*\left(\int_{t-s}^{t} x_q d\mu q\right)^2$$

$$= \mu \int_{t-s}^{t} E^* x_q^2 dq + \mu^2 E^*\left(\int_{t-s}^{t} x_q dq\right)^2 \qquad \text{-------- (15)}$$

$$= \mu \int_{t-s}^{t} B(q)dq + \mu^2 E^*\left(\int_{t-s}^{t} x_q dq\right)^2 . \cdot$$

To compute $E^*\left(\int_{t-s}^{t} x_q dq\right)^2$, we take the derivative of $\left(\int_{t-s}^{t} x_q dq\right)^2$ and then integrate it:

$$d\left(\int_{t-s}^{t} x_q dq\right)^2 = 2\int_{t-s}^{t} x_q dq\,(x_t - x_{t-s})dt$$

$$= 2\int_{t-s}^{t} (x_q x_t - x_q x_{t-s})dq\ dt\,, \qquad \text{------- (16)}$$

$$\left(\int_{t-s}^{t} x_q dq\right)^2 = 2\int_{0}^{t}\int_{v-s}^{v} (x_q x_v - x_q x_{v-s})dq\ dv + \left(\int_{-s}^{0} x_q dq\right)^2$$

$$= 2\int_{0}^{t}\int_{v-s}^{v} (x_q x_v - x_q x_{v-s})dq\ dv + \int_{-s-s}^{0\ 0}\int x_q x_v dqdv\ .$$

Now take the expectation under risk-neutral probability, we have that

$$E^*\left(\int_{t-s}^{t} x_q dq\right)^2 = 2\int_{0}^{t}\int_{v-s}^{v} (C(q,v) - C(q,v-s)dq\ dv + \int_{-s-s}^{0\ 0}\int C(q,v)dq\ dv \qquad \text{-------- (17)}$$

$$= F(t,s) + H\,,$$

Where $F(t,s) = 2\int_{0}^{t}\int_{v-s}^{v} (C(q,v) - C(q,v-s)dq\ dv$

and $H = \int_{-s-s}^{0\ 0}\int C(q,v)dq\ dv\,.$

Taking into account (14), (15), and (17), equation (13) becomes

$$\frac{dy(t)}{dt} = \beta U + \frac{\gamma}{s}\left[\int_{t-s}^{t} y(q)dq + \mu\int_{t-s}^{t} B(q)dq + \mu^2(F(t,s)+H) + (\lambda - r)^2 s^2 - 2\mu s(\lambda - r)\int_{t-s}^{t} A(q)dq\right] - (\gamma + \beta)y(t).$$

--------- (18)

We can check that (2) is a special case of (18) with

$A(t) = E[x_t] = \sigma$, $B(t) = E[x_t^2] = Var\,[x_t] + (E[x_t])^2 = \delta + \sigma^2$, and

$C(q,t) = E[x_q x_t] = E[x_q]E[x_t] = \sigma^2$.

To get the expectation of the realized variance in the risk-neutral world $E^*[y]$, we have to find a solution to (18) a nonhomogeneous integrodifferential equation with delay.
After taking the first derivative of this equation, we obtain

$$y''(t) = \frac{\gamma}{s}[y(t) - y(t-s)] - (\gamma + \beta)y'(t) + h(t,s), \qquad \text{------- (19)}$$

Where $h(t,s) = \left(\frac{\gamma}{s}\right)\left[\mu(B(t) - B(t-s)) + \mu^2 F'(t,s) - 2\mu s(\lambda - r)(A(t) - A(t-s))\right]$.

This is a second – order delay differential equation with constant coefficients, and so Laplace transform can be applied to find its solution with initial condition $y(t) = \rho(t, Q_t),\ t \in [-s, 0]$, , which is already known [8], [19].

Let us denote the Laplace transform of a function f (t)as

$$L\{f(t)\} = \int_0^\infty f(t)e^{-qt}dt \qquad \text{------ (20)}$$

and do the Laplace transform for (19)

$$L\{y''(t)\} = \frac{\gamma}{s}[L\{y(t)\} - L\{y(t-s)\}] - (\gamma + \beta)L\{y'(t)\} + L\{h(t,s)\} \qquad \text{----- (21)}$$

By change of variable and the property of Laplace transform, 19 yields

$$\left[q^2 + (\gamma + \beta)q - \frac{\gamma}{s}(1 - e^{-qs})\right]L\{y(t)\} = y'(0) + (q + \gamma + \beta)y(0) - \frac{\gamma}{s}e^{-qs}\int_{-s}^{0} y(t)e^{-qt}dt + L\{h(t,s)\}.$$

------ (22)

The characteristic function of 17 is

$$C(q) = q^2 + (\gamma + \beta)q - \frac{\gamma}{s}(1 - e^{-qs}) \approx q^2 + \beta q \ . \qquad \text{------- (23)}$$

Therefore,

$$L\{y(t)\} = C^{-1}(q)\left[y'(0) + (q + \gamma + \beta)y(0) - \frac{\gamma}{s}e^{-qs}\int_{-s}^{0} y(t)e^{-qt}dt + L\{h(t,s)\}\right] . \qquad \text{-------- (24)}$$

Applying the inverse transform 19, we have that

$$y(t) \approx \frac{1 - e^{-\beta t}}{\beta}y'(0) + \left[\frac{\gamma}{\beta}(1 - e^{-\beta t}) + 1\right]y(0) - \frac{\gamma}{\beta s}\int_{-s}^{0} y(q)[1 - e^{-\beta(t-q-s)}]dq + \frac{1}{\beta}\int_0^t h(q,s)[1 - e^{-\beta(t-q)}]dq + C.$$

------- (25)

By the initial condition,

$$C = \frac{\gamma}{\beta s}\int_{-s}^{0} y(q)[1 - e^{-\beta(q+s)}]dq \ . \qquad \text{------ (26)}$$

Hence, the expectation of the realized variance for compound Poisson jump under risk-neutral measure P* can be obtained by

$$F_{\text{var}} = E^*[y] = \frac{1}{W}\int_0^W y(t)dt, \qquad \text{------ (27)}$$

III. EXAMPLE

The Fig. (1) shows the GIP responses after oral glucose tended to be lower in the type-2 diabetic patients as defined in [13]. With high rate of GIP infusion, a greater insulin secretary response was elicited in normal subjects, but in type-2 diabetic even the pharmacological concentrations of GIP reached only marginally stimulated insulin secretion. Whereas in normal subjects the glucose infusion had to be increased owing to GIP-stimulated insulin release, the glucose infusion rate hardly had to be increased in type-2 diabetic patients.

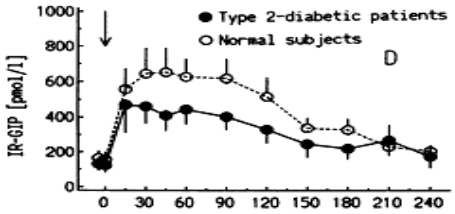

Fig. (1)

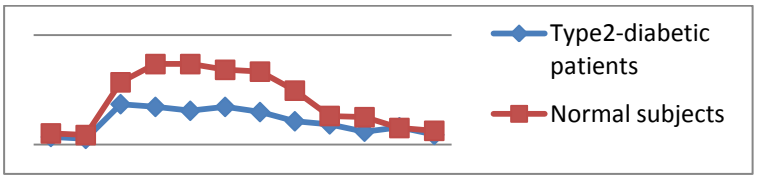

Fig. (2)

IV. CONCLUSION

Evaluation of the GIP response after oral glucose tended to be lower in the type-2 diabetic patients than normal subjects fitted with the characteristic equation obtained by applying Laplace transform to the second order delay differential equation with jump represented by compound Poisson process is graphically shown in Fig(2). The result coincides with the mathematical and medical report.

REFERENCES

[1]. Anatoliy swishchuk and Li xu, Pricing variance swaps for stochastic volatilities with Delay and Jumps. Vol 2011, Article ID 435145.
[2]. Buchan, A. M. J., J. M. Polak, C. Capella, E. Solcia and A. G. E. Pearse. 1978. Electronimmunocytochemical evidence for the K cell localization of gastric inhibitory polypeptide (GIP) in man. Histochemistry. 56:37-44.
[3]. Creutzfeld, W. 1979. The incretin concept today. Diabetologia.16:75-85.
[4]. Creutzfeldt, W., R. Ebert, M. Nauck, and F. Stockmann. 1983. Disturbances of the entero-insular axis. Scand. J. Gastroenterol. Suppl. 83:111-119.
[5]. D. Lamberton and B. Lapeyre, Introduction to Stochastic calculus applied to finance, Chapmann & Hall, London, U.K, 1996.
[6]. Dupre, J., S. A. Ross, D.Watson, and J. C. Brown. 1973. Stimulation of insulin secretion by gastric inhibitory polypeptide in man. J. Clin. Endocrinol. Metab.37:826-828.
[7]. Fuessl, H.S., Y. Yiangou, M. A. Ghatei, F.D. Goebel, and S. R. Bloom. 1990. Effect of synthetic human glucose-dependent insulinotropic polypeptide(hGIP) on the release of insulin in man. Eur. J. Clin. Invest. 20:525-529.
[8]. J.K. Hale and S. M. Lunel, Introduction to Functional-Differential Equations, vol. 99 of Applied Mathematical Sciences, Springer, NewYork, NY, USA, 1993.
[9]. Jones, I. R., D. R. Owens, A. J. Moody, S. D. Luzio, T. Morris, and T. M. Hayes.1987. The effects of glucose-dependent insulinotropic peptide infused at physiological concentrations in normal subjects and type 2 (non-insulin-dependent) diabetic patients on glucose tolerance and B-cell secretion. Diabetologia. 30:707-712.
[10]. Jornvall, H., M. Carlquist, S. Kwauk, S. C. Otte, C. H. S. McIntosh, J. C. Brown, and V. Mutt. 1981. Amino acid sequence and heterogeneity of gastric inhibitory polypeptide (GIP). FEBS(Fed. Eur. Biochem. Soc.) Lett. 123:205-210.
[11]. Krarup, T. 1988. Immunoreactive gastric inhibitory polypeptide. Endoct. Rev. 9:122-134.
[12]. krarup, T., N. Saurbrey, A. J. Moody, C. Kuhl, and S. Madsbad. 1987. Effects of porcine gastric inhibitory polypeptide on beta-cell function in type1 and II diabetes mellitus. Metab. Clin. Exp. 36:677-682.
[13]. Michael A. Nauck, Markus M. Heimesaat, Cathrine Orskov, Jens J. Holst, Reinhold Ebert, and Werner Creutzfeldt. Preserved incretin activity of Glucogan-like peptide 1 [7-36 Amide] buy Not of synthetic Human Gastric inhibitory Polypeptide in patients with Type 2 – Diabetes Mellitus.
[14]. Moody, A. J., L. Thin, and I. Valverde, I. 1984. The isolation and sequencing of human gastric inhibitory polypeptide (GIP). FEBS(Fed. Eur. Biochem. Soc.) Lett.172:142-148.
[15]. Nauck, M. A., E. Homberger, E.G. Siegel, R.C. Allen, R.P. Eaton, R. Ebert, and W. Creutzfeldt. 1986. Incretin effect of increasing glucose loads in man calculated from venous insulin and C-peptide responses. J. Clin. Endocrinol. Metab.63:492-498.
[16]. Nauck, M., F. Stockmann, R. Ebert, and W. Creutzfeldt.1986. Reduced incretin effect in type-2 (non-insulin-dependent) diabetes. Diabetologia 29:46-52
[17]. Nauck, M., W. Sehmidt, R. Ebert, J. Strietzel, P. Cantor, G. Hoffmann, and W. Creutzfeldt. 1989. Insulinotropic properties of synthetic human gastric inhibitory polypeptide in man: interactions with glucose, phenylalanine, and cholecystokinin 8. J. Clin. Endocrinol. Metab.69:654-662.
[18]. Perley, M.J., and D.M. Kipnis. 1967. Plasma insulin responses to oral and intravenous glucose: studies in normal and diabetic subjects. J. Clin. Invest.46:1954-1962.
[19]. R. Bellman and K. L. Cooke, Differential-Difference Equations, Academic Press, NewYork, NY, USA, 1963.
[20]. Tronier, B., A. Deigard, T. Andersen, and S. Madsbad. 1985. Absence of incretin effect in obese type2 and diminished effect in lean type2 and obese subjects. Diabetes Res. Clin. Pract. (Suppl.1) S568.(Abstr.).

ISSN (e): 2250 – 3005 || Volume, 05 || Issue, 07 || July – 2015 ||
International Journal of Computational Engineering Research (IJCER)

Convection interaction in GaAs/LEC growth model

Reza Faiez[1], Farzad Najafi[2], Yazdan Rezaei[1]
[1] Solid State Lasers Research Group, School of Laser and Optics, Tehran, P.O.Box 11365-8486, Iran
[2] Research Institute of Petroleum Industry (RIPI), Tehran, P.O.Box 14665-137, Iran

ABSTRACT:
Fluid flow and heat transport are investigated for the GaAs melt rotating with its cylindrical container in a liquid encapsulated Czochraslki (LEC) growth system in which the flow pattern and temperature distribution in the melt are influenced by coupling of rotationally–driven forces to the thermal convection. The experimentally observed particular shape of the crystallization front was predicted numerically. The convective flow in the melt was studied by focusing on the Rayleigh-Benard and the baroclinic instabilities. Increasing the crucible rotation rate, the dominant convective cell found to pivot by a small angle in the meridional plane around the vorticity vector. This pivoting angle is directly related to the Ekman shear angle.

Keywords: *Computer simulation, Convection, Flow pattern, Coriolis forces, Interfaces, LEC growth*

I. INTRODUCTION

Low Prandtl-number ( ) semiconductor melt in a modified Czochralski (Cz) puller [1, 2] can be modeled as a two-dimensional Boussinesq fluid which rotates uniformly with its container. In the absence of an applied electromagnetic field, hydrodynamic processes relevant to crystal growth are classified into the following main groups: natural gravitational type convection, forced convection and the surface-tension driven convection. Typically, hydrodynamics and the associate transport phenomena in the system are quite complex because of their highly nonlinear and strong coupled interactions [3, 4]. The crystal quality is closely related to the crystallization front shape which depends on the heat balance at the vicinity of the front. Associated with a curved (convex or concave to melt) phase interface, the radial non-uniformity of the thermal history affects the crystal structure due to the formation of facets on the oxides growth interface [5]. In the case of semiconductors such as GaAs and InP, the density of the dislocations is a direct consequence of thermal stress in the crystal during the process. The maximum stresses which occur at the crystal periphery were found [6, 7] to be related to the growth interface morphology. The gull-winged shape GaAs phase boundary, revealed by different model calculations [8, 9], is well supported by experimental data [10, 11]. This typical interface shape, concave to melt ( ) at periphery and convex ( ) to melt in the center, strongly depends on the flow field structure [12]. Therefore, the interface destabilization, leading to thermal stresses and high dislocation density in the crystal, is mainly due to the convective instabilities in the melt.

Hydrodynamic stability, concerning the stability and instability of the fluid motions, has been largely studied in the last decades [13, 14]. Experimental data on the regime diagram of different fluids, each contained in a rotating cylindrical annulus and subjected to an imposed radial temperature gradient, were reported first by Fein and Pfeffer [15]. Their results were summarized in the form of two-parameter diagrams (thermal Rossby number vs. Taylor number) for different Pr numbers. For moderate and low Pr-number fluids, namely water ( ) and mercury ( ), they have displayed the well-known knee type (or the anvil shape) diagrams which characterize the transition from axisymmetric flow to regular baroclinic waves. The anvil-shape regime diagram for moderate Pr-number fluid, apart from the baroclinic regular wave, revealed the upper and the lower symmetric regimes. While the flow in the lower one is established by diffuse effects, the axisymmetric flow in the upper symmetric regime is stable due to stratification.

Though geometry of Cz configuration is different from the rotating annulus experiments, similarity of the flow field structure in between has been paid much attention [16, 17]. Compared to moderate and high Pr-number fluids, studies on hydrodynamic stability of low Pr-number Cz-melts (Si, GaAs, InP), initiated by Ristorcelli and Lumley [16] and Kakimoto [17], appears to be scare. This is more pronounced in the case of GaAs melt for which the convective flow was studied by Polezahaev et al [18]. Using an axisymmetric modeling of fluid flow without a swirl, the critical Grashof number was estimated to be as high as ~ for GaAs/Cz system of the aspect ratio [18]. They have shown that the critical number for the onset of thermal oscillations in the melt decreases to ~ when the melt depth increased, namely for . However, it is well-known [19] that for a low Pr melt rotating with its container, the critical Rayleigh number increases with the rotation rate. The so-called overstability associated with rotation intensity, namely the Taylor number, is an important feature of convection with rotation [20].

The main purpose of the present work is to investigate the flow field structure of the GaAs/Cz melt. The effect of rotationally driven- and thermocapillary forces on the flow pattern is studied. Both rotating Rayleigh-Bénard instability [21, 22] and the baroclinic instability [17, 23] are to be considered. The mathematical model developed in the present study incorporates transport processes of all domains of the system. The crystal is considered to be passive here and serves the purpose of enforcing an isothermal boundary condition at the crystallization front.

II. MODEL DESCRIPTION AND NUMERICAL SCHEME

2.1. Physical Model and Basic Assumptions

The idealized geometry of a modified Cz puller, the computational domains and the coordinate system adopted in the present analysis are illustrated in figure 1. The system is assumed to be in a pseudo-steady state and the axi-symmetric. Continuity, Navier-Stokes and energy equations are solved with the Boussinesq approximation. Both the GaAs melt and the encapsulant are incompressible Newtonian fluids with laminar flows. Thermophysical properties of the system are constant except for the temperature-dependency of the encapsulant dynamic viscosity, μ_e. The crucible bottom is thermally insulated and its side wall of height (h_m+h_e) is at a uniform and constant temperature, T_c. The physical properties of the system used for simulations are given in reference [24]. The thermophysical properties of ambient gas (Argon) are summarized in Table 1. The geometrical as well as the process parameters used in the present simulations are given in Table 2.

Table 1: Physical properties of Gas used for simulations

Density, ρ_g	486.8295/T kg/m^3
Thermal conductivity, λ_g	0.01+(2.5×10^{-5}) ×T W/m.K
Specific heat, c_{Pg}	521 J/kg.K
Dynamic Viscosity, μ_g	8.466×10^{-6} + 5.365×10^{-8} T- 8.682×10^{-12} T^2

Table 2: Geometrical and process parameters used for simulation

Crucible radius, r_c	0.075 m
Crystal radius r_s	0.0375 m
Melt height, h_m	0.05 m
Encapsulant height, h_e	0.02 m
Insulating enclosure height, h_E	0.2 m
Characteristic length	L=[h^4_m/(r$_c$-r$_s$)]$^{1/3}$
Crystal height, h_s	0.12 m
Crystal rotational rate, Ω_x	5 rpm
Crucible rotational rate, -Ω_c	5-20 rpm
Pulling rate, u_p	10 mm/h
Crucible wall temperature, T_c	1529 K
Enclosure top temperature, T_a	1261 K
Insulating enclosure emissivity, ε_E	0.8

In this configuration, the counter rotation of the crystal $(r_s;\Omega_x)$ and crucible $(r_c;-\Omega_c)$ influences the flow field in the melt. In the present study, a set of numerical simulations was performed for a 37.5mm radius crystal, 75mm radius crucible and 50mm height melt. Hence, the ratio between the Reynolds numbers Re_c and Re_s equals to $4\left|\Omega_c/\Omega_x\right|$ by definition of $\mathrm{Re} = r^2\Omega/\nu$. Throughout the calculations, Ω_x is assumed to be constant and equal to a reasonably [25] small value $(5\ rpm \cong 0.524\ rad/s)$ while the crucible rotation rate varies from -5 to -20 rpm.

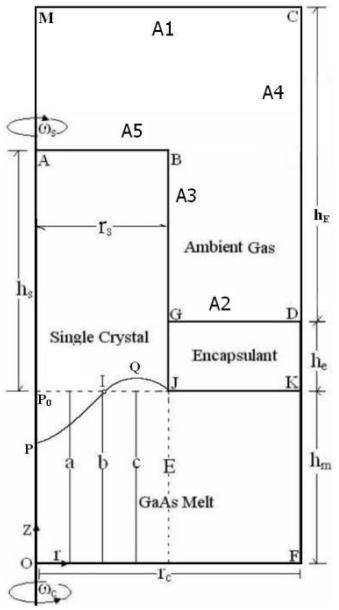

Figure 1: Sketch of a modified Czochralski crystal growth setup and the computational domains. The curve PIJ represents the M-type experimental interface shape on which the point I is the inflection point.

2.2. Mathematical Model

Throughout the present simulations, the Reynolds number of the GaAs melt flow field $\mathrm{Re}_m = u_{\max} L / \nu$, does not exceed the computationally obtained [25] Re_x^* and/or Re_c^* values. This may ensure the validity of the axisymmetric flow assumption in the present modeling. Therefore, all variables $\Phi = \Phi(r, z)$ in Table 3 are independent of the azimuthal θ angle and the numerical model solves three momentum equations for three velocity components, u_r, u_z and u_θ in two-dimensional space. The variations in the fluid density are ignored except insofar as their effect on the gravitational force.

Table 3: The diffusion coefficient Γ_Φ and source term S_Φ for variable Φ

Φ	Γ_Φ	S_Φ
1	0	0
u_z	μ	$-(\partial p/\partial z) + \rho g \beta (T - T_{ref})$
u_r	μ	$-(\partial p/\partial r) - \mu u_r / r^2 + \rho u_\theta^2 / r$
u_θ	μ	$-\mu u_\theta / r^2 - \rho u_r u_\theta / r$

Based on these assumptions, the generalized transport equation (GTE), governing the fluid flow and heat transfer in this arrangement, can be expressed in polar-cylindrical coordinate system as

$$\frac{\partial}{\partial z}(\rho u_z \Phi) + \frac{1}{r}\frac{\partial}{\partial r}(\rho r u_r \Phi) = \frac{\partial}{\partial z}\left(\Gamma_\Phi \frac{\partial \Phi}{\partial z}\right) + \frac{1}{r}\left(r\Gamma_\Phi \frac{\partial \Phi}{\partial r}\right) + S_\Phi \,, \qquad (1)$$

for which the diffusion coefficient Γ_Φ and the source term S_Φ for dependent variables Φ are listed in Table 3. The first and the last rows in Table 3 are the expressions of continuity and the energy equations, respectively. The energy loss due to viscous dissipation is neglected. T_{ref} is the reference temperature for the Boussinesq approximation, p the reference pressure, β the coefficient of volumetric expansion and g is the gravitational acceleration constant.

In the present cylindrical model, the streamline function ψ and vorticity ω are defined in terms of the radial and axial velocities as $u_r = -(1/r)(\partial\psi/\partial z)$, $u_z = (1/r)(\partial\psi/\partial r)$ and $\omega = \partial u_r/\partial z - \partial u_z/\partial r$. Physically ψ is a measure of the volume flux. So the difference between the values of ψ at two points in the meridional plane is proportional to the meridional flux between them. The vorticity is associated with rotational motion and in a 2D flow the vorticity vector is orthogonal to the plane of flow.

2.3. Boundary conditions

Corresponding to the boundaries defined in figure 1, the conditions applied to the system are listed in Table 4. Altogether, three types of flow boundary conditions were used for the whole set of computations: no slip boundary for the crucible, crystal and insulator, no shear stress on symmetry axis and Marangoni boundary condition for both the encapsulant free surface and the melt/encapsulant interface. The numerically approximated temperature [24] at the crucible side wall ($0 < z < (h_m + h_e)$) was employed as a constant. Corresponding to the heat input around 1.5 kW in the case of mixed convection, T_c=1529 K is suitable for growth of 3″ diameter GaAs crystal providing the pull rate ~ 10-15 mm/h in the growth process. The crucible bottom is insulated and assumed to be adiabatic. Above the crucible top end, the temperature of the insulating enclosure wall, T_E is assumed to be variant as given in Table 4. The top enclosing wall is at the same temperature as the ambient T_a=1261 K. Both the temperatures along the crucible bottom and the enclosure top surface are of considerable importance for the control of the GaAs/Cz process, particularly for the shape of CMI.

Table 4: The applied boundary conditions corresponding to Figure 1.

	u_z	u_r	u_θ	T
OP_0	$\frac{\partial u_z}{\partial r} = 0$	0	0	$\frac{\partial T}{\partial r} = 0$
AP_0	u_P	0	0	$\frac{\partial T}{\partial r} = 0$
AB	0	0	$r\,\Omega_x$	$-\lambda_s \frac{\partial T_s}{\partial z} = h_{sg}(T_s - T_a) + \varepsilon_s \sigma (T_s^4 - T_{eff}^4)$
AM	0	0	0	$\frac{\partial T}{\partial r} = 0$
MC	0	0	0	T_a
DC	0	0	0	$T_z = (T_C - T_a)\left[\frac{h_E - h_z}{h_E}\right]^6 + T_a$
KD	0	0	$r_C\Omega_C$	T_c
FK	0	0	$r_C\Omega_C$	T_c
OF	0	0	$r\,\Omega_C$	$\frac{\partial T}{\partial z} = 0$
JK	0	$\mu_m \frac{\partial u_r}{\partial z} = \frac{\partial \gamma_m}{\partial T}\frac{\partial T_m}{\partial r}$	$\frac{\partial u_\theta}{\partial z} = 0$	$-\lambda_m \frac{\partial T_m}{\partial z} + \lambda_e \frac{\partial T_e}{\partial z} = \alpha_e \varepsilon_m \sigma (T_m^4 - T_{eff}^4)$
JG	u_P	0	$r_x\Omega_x$	$-\lambda_s \frac{\partial T_s}{\partial r} + \lambda_e \frac{\partial T_e}{\partial r} = \alpha_e \varepsilon_s \sigma (T_s^4 - T_{eff}^4)$
GB	u_P	0	$r_x\Omega_x$	$-\lambda_s \frac{\partial T_s}{\partial r} = h_{sg}(T_s - T_a) + \varepsilon_s \sigma (T_s^4 - T_{eff}^4)$
GD	0	$\mu_e \frac{\partial u_r}{\partial z} = \frac{\partial \gamma_e}{\partial T}\frac{\partial T_e}{\partial r}$	$\frac{\partial u_\theta}{\partial z} = 0$	$-\lambda_e \frac{\partial T_e}{\partial z} = h_{eg}(T_e - T_a) + \varepsilon_e \sigma (T_e^4 - T_{eff}^4)$

The effective temperature, $T_{eff,\,k}$ which appears in Table 4, is due to radiative heat exchange in the present system. According to the Gebhart theory of radiation, the net radiative heat exchange between an exposed surface k at temperature T_k, and all others in an N-sided enclosure can be calculated as:

$$q_k = \varepsilon_k \sigma T_k^4 - \frac{1}{A_k}\sum_{i=1}^{N} G_{ik}\,\varepsilon_i \sigma T_i^4 A_i = \varepsilon_k \sigma (T_k^4 - T_{eff,k}^4) \qquad (2)$$

Where A_k is the area of the surface k and

$$T_{eff,k} = \left(\frac{1}{A_k \varepsilon_k}\sum_{i=1}^{N} A_i \varepsilon_i G_{ik} T_i^4\right)^{1/4} \qquad (3)$$

is the effective temperature to which the surface k loses heat by radiation. The Gebhart factor,

$$G_{ik} = F_{ik}\varepsilon_k + \sum_{j=1}^{N} F_{ij}(1-\varepsilon_j) G_{jk} \qquad (4)$$

represents the fraction of out-going flux from surface i that absorbed by surface k. The calculation procedure for the view factor matrix F(i,j) is straightforward for meniscus free surface. The above set of linear equations for G_{ik} (i, k =1,2,…,N) can be solved by Gaussian elimination. Repeating the calculations for all surfaces by changing k, one obtains all the Gebhart factors. For N=5 flat-zones enclosure in the present configuration, the number of independent view factors to be determined is only (N/2)(N-3)=5.

2.4. Numerical model

The two-dimensional differential equations (1) with the boundary conditions for the fluid flow and heat transport in the Cz configuration were solved numerically by the finite volume method (FVM). The computational domain was discretized into a finite number of control volumes over which the governing equations were integrated. The resulting system of algebraic equations was solved iteratively until convergence was reached. A staggered grid system was employed for different dependent variables. The pressure p, the azimuthal velocity u_θ, and the temperature T were calculated at the grid point in the center of the main control volume (MCV); the axial and radial components of velocity u_z and u_r, respectively, were staggered in the z and r directions to the mid-point of the boundaries of MCV. The SIMPLEC algorithm [26] was used to couple velocities and pressure on staggered grids. The grid used in the present calculation is uniform for the computational domain of melt, encapsulant, crystal and the ambient gas. It contains 52×272 grid points with spacing of $1.0\,mm$ resulting in a grid-independent solution. For all variables Φ, the solution was deemed convergent when the criterion $\left|\Phi^{n+1} - \Phi^{n}\right|_{\max} \le 10^{-4}$ was satisfied where n represents the index of iteration number. The accuracy of the numerical code was ascertained by validating the general results of the present calculation with the experimental [11, 27] and 2D numerical [6, 9] results obtained for corresponding geometry and boundary conditions. Remarkable is the particular shape of CMI which appears in the present simulations as obtained in the model analyses of both liquid encapsulated Czochralski and VCz growth of GaAs bulk crystals.

III. RESULTS AND DISCUSSION

In this section, the nature of the GaAs/Cz melt convective flow is described. The results obtained from the numerical simulations are presented. The influence of rotationally-driven forces on the flow field structure and temperature distribution is discussed.

3.1. Description of the flow field structure

The convection instabilities in Czochralski melt are among the most challenging issues in bulk crystal growth modeling. This is mainly due to the complexity of hydrodynamics and associated heat transport in the melt from which a crystal is growing. In the present model, the flow instability can exhibit unique features because of coexisting vertical nad horizontal temperature gradients and the differential rotation rates of the crystal ($r_x ; \Omega_x$) and crucible ($r_c ; -\Omega_c$). The minus sign here means the counter-clockwise direction of rotation. For a liquid rotating with its container, besides the gravity, it is necessary to include two body forces, the centrifugal force representing a vector derivative $\boldsymbol{\Omega}_c \wedge (\boldsymbol{\Omega}_c \wedge \mathbf{r})$ and the Coriolis force $2(\boldsymbol{\Omega}_c \wedge \mathbf{u})$ with $\mathbf{r}$ and $\mathbf{u}$ as the position and velocity vectors, respectively. The effects of centrifugal force are usually neglected in model calculations, particularly for the crystal growth set-ups, and the analysis has largely been restricted to consideration of the interaction between the Coriolis and buoyancy forces. In the GaAs melt, the natural convection may readily become unsteady and time-dependent because of its low Pr number. Even with small driving temperature differences, $\Delta T_{\max} = 18\,K$ imposed on the system ($h_m / r_c = 0.67$), the Grashof number Gr_m was found to be of order 10^7. However, compared to its critical number calculated for 2D melt without a swirl [18], the flow may be assumed to be axisymmetric in the present model in which the melt is rotating with its container.

The crystal rotation generates an upward flow in the melt central column which encounters the large-scale circulation (LSC) caused by the crucible rotation in the same direction as the buoyancy and thermocapillary convections. In the configuration with $\mu < 0$ as the rotation ratio $-\Omega_c / \Omega_x$ and the radius ratio of $\eta = r_x / r_c = 0.5$, this can be readily verified that $\mathrm{Re}_c / \mathrm{Re}_x = 4\mu$. With a constant and reasonably small [25] $\Omega_x = 0.524\ rad/s$ throughout the calculations, the large-scale flow was found to be the dominant feature of the flow pattern. The parameter $\mathrm{Ra}/\mathrm{Pr}.\mathrm{Re}_c^2$ is so high (~10), compared to $\mathrm{Ra}/\mathrm{Pr}.\mathrm{Re}_x^2$ that the upward central flow does not appear in the present simulations. In fact, only for $\Omega_c \le 0.417\ rad/s$ (~4.0 rpm), the governing parameter $(\mathrm{Ra}/\mathrm{Pr}.\mathrm{Re}_c^2) \ge 1$ can be held. Hence, the reason for an eventual instability in the system is coupling of thermal convection and the forces generated by the crucible rotation. Furthermore, the surface tension to buoyancy ratio $\mathrm{Ma}/\mathrm{Pr}.\mathrm{Gr}^{1/2}$ for the GaAs melt is large enough (~180 compared to ~120 in[16] for Si) to modify the structure of the flow. However, as illustrated in figure 2, the effect is strongly controlled by the presence of highly viscous ($\mu_e / \mu_m \sim 10^3$) encapsulated layer on the GaAs melt surface. Far from the melt/encapsulant boundary, the flow velocity vectors and temperature profiles in the melt are influenced by

thermocapillary forces. This effect leads to a more convex to melt interface by changing slightly the direction of the velocity vectors in peripheral part of the phase boundary. The flow velocity vectors close to the melt/encapsulant interface were found to be so small (see figure 2) and the flow remained in a steady state as assumed in the present model. This can be inferred that, for the GaAs melt/encapsulant system, the effective critical Ma number should be far beyond the estimated $\sim 6.9 \times 10^{4} (\mathrm{Pr})^{1.36}$ value [28] for low Pr melts.

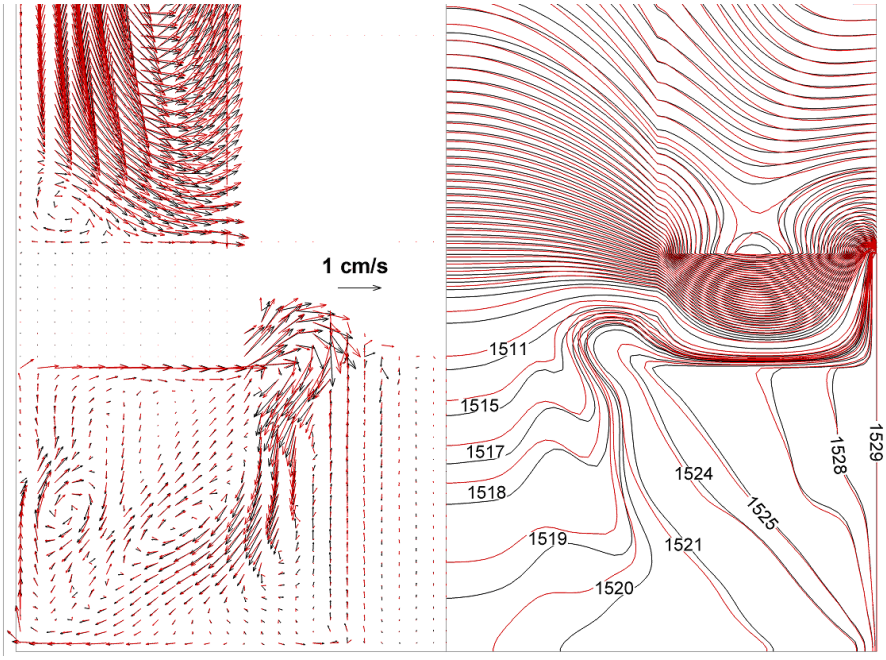

Figure 2: Marangoni effect (black lines) on the velocity field (left) and temperature distribution (right). The rotation rates for crystal and crucible are +5 and -5 rpm, respectively.

For the GaAs melt in a rotating Cz crucible, the Coriolis force largely influences the buoyancy-driven flow due to coupling of the radial velocity with the fluid rotation. Though the Coriolis force stabilizes the fluid flow due to the prevention of vertical convection, it complicates however the structure of the flow field by increasing the curvature the fluid particle-paths. Therefore, hydrodynamics of the GaAs melt in a non-inertial frame is characterized by the Taylor number T_a and thermal Rossby number Ro_T. By definition Ta stands for the ratio of Coriolis force to the viscous force, and the Rossby number is the ratio between convective acceleration and the Coriolis force. Non-dimensional parameters related to the present model are given in Table 5.

Table 5. Dimensionless similarity parameters for the GaAs melt convection with the rotation. The characteristic length $L = 5.503 \times 10^{-2}\, m$, $\Delta T_{\max} = 18\, K$, $\Omega_x = 0.524\ rad/s$ and $\Omega_x \le \Omega_c \le 2.094\ rad/s$.

$\mathrm{Ra} = (g\beta/\nu\alpha) L^3 \Delta T_{\max}$	1.574×10^{6}
$\mathrm{Ma} = (\gamma_T/\mu\alpha) L \Delta T_{\max}$	5.928×10^{4}
$\mathrm{Re}_x = r_x^2 \Omega_x / \nu$	1.511×10^{3}
$\mathrm{Re}_c = r_c^2 \Omega_c / \nu$	$1.153 \times 10^{4} \Omega_c$
$\mathrm{Ta} = 4\Omega_c^2 (r_c - r_x)^5 / \nu^2 L^2$	$2.744 \times 10^{7} \Omega_c^2$
$\mathrm{Ro}_T = g\beta \Delta T_{\max} L / \Omega_c^2 (r_c - r_x)^2$	$1.292 / \Omega_c^2$

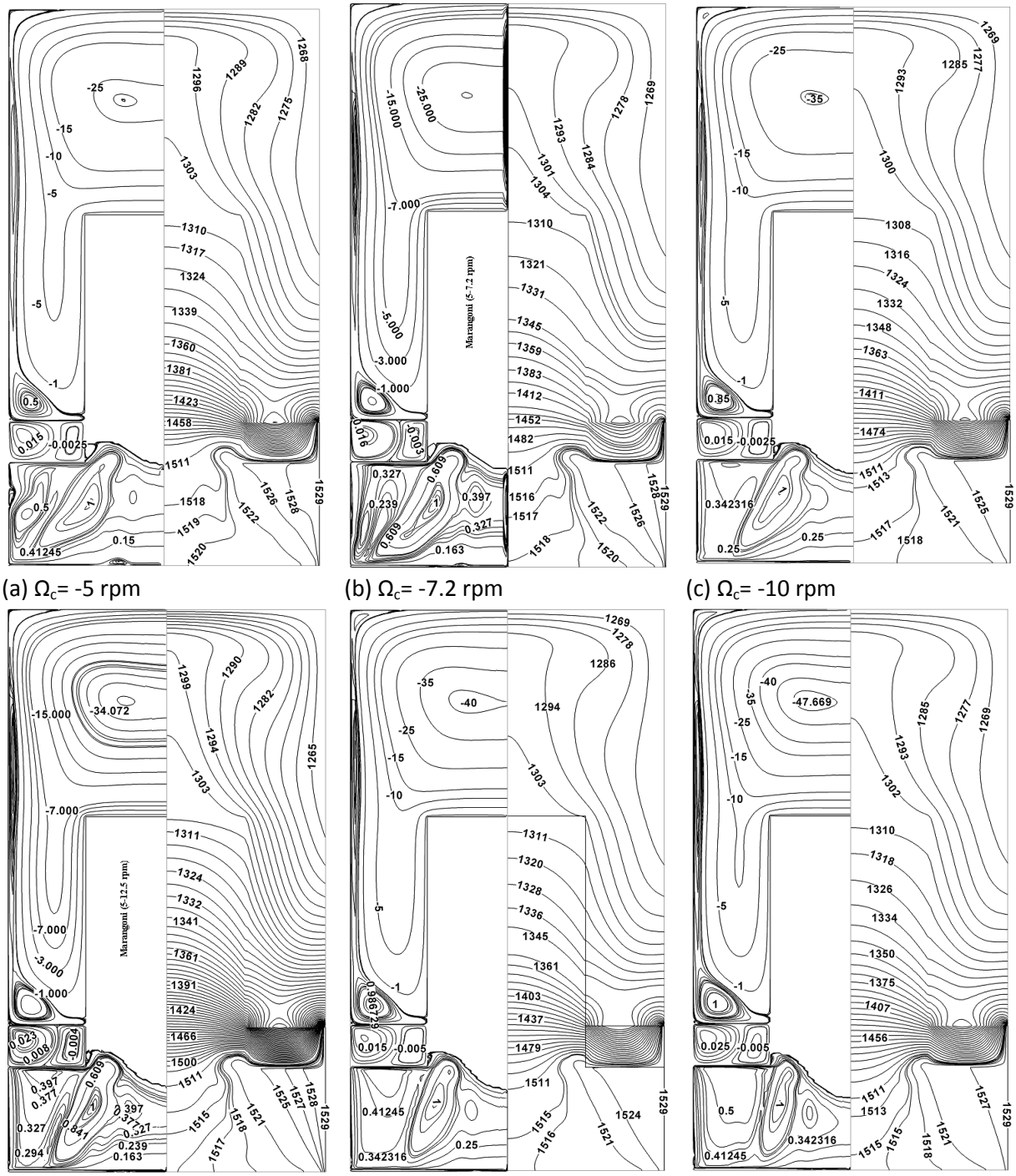

(a) Ω_c= -5 rpm (b) Ω_c= -7.2 rpm (c) Ω_c= -10 rpm

(d) Ω_c= -12.5 rpm (e) Ω_c= -15 rpm (f) Ω_c= -20 rpm

Figure 3 (a-g): Contours of stream function (left) and temperature (right) with $\mathrm{Ra} = 1.574 \times 10^{6}$, $\mathrm{Ma} = 5.928 \times 10^{4}$, $\mathrm{Re}_x = 1.511 \times 10^{3}$ for different crucible rotation rates.

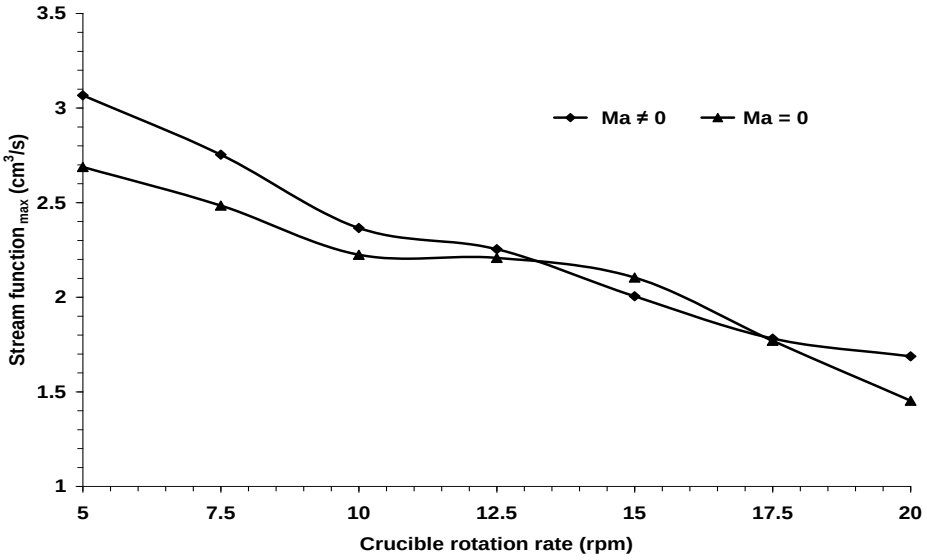

Figure 4: Maximum intensity of the convection as a function of the rotation rate.

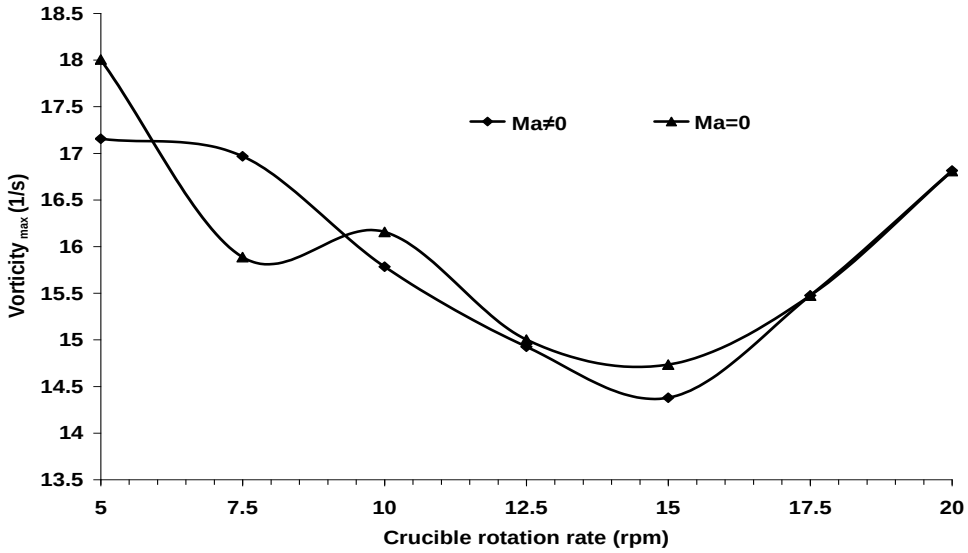

Figure 5: Maximum vorticity of the flow as a function of the rotation rate.

3.2. Simulation of the flow field and temperature distribution

In the GaAs melt rotating with its container, the flow field and heat transport are influenced by the impact of Coriolis force on the thermal convection flow. The flow field and temperature distribution are illustrated in figure 3 (a-g) for the melt characterized by $\mathrm{Ra}_m = 1.574 \times 10^6$, $\mathrm{Ma} = 5.928 \times 10^4$, $\mathrm{Re}_x = 1.511 \times 10^3$. The crucible rotation varies in the range $0.524 \le |\Omega_c| \le 2.094\ rad/s$. To describe the multi-cell structure of the flow, the line b ($r = r_x/2$, $z = h_m$), crossing approximately the inflection point (I) on the phase boundary, and the line E as the edge of the melt central column (see figure 1) are used.

As for any rotating stratified fluid in a container [20] the structure of the flow is dominated by a centrifugally-driven large-scale circulation (LSC). The roll (LSC) is characterized by $\psi(r,z)/\psi_{\max} = 1$ and found to be headed towards the peripheral concave to melt part of the phase interface. For all cases, the central position of LSC lies approximately on the edge E nearby the point M_i ($r = r_c/2$, $z = h_m/2$) in the interior of the melt. As shown in figure 3 (a-g), at lower rotation rates $|\Omega_c| \le \Omega_x$ the dominant cell is tailed to the corner and compressing the buoyancy driven flow near the wall makes a tilt angle θ_ψ with respect to the vertical line E.

Increasing $|\Omega_c|$, the LSC rotates around the vortex vector $\boldsymbol{\omega}_{\max}$ so that θ_ψ decreased and the buoyancy driven convection is expanded and the flow pattern between the wall and the edge, E is considerably simplified.
Figure 4 shows that the intensity of the convection, $\psi_{\max}$ strongly depends on the rotation rate. Coupling to the radial velocity of the flow, the Coriolis force enhancement has a restrictive effect on the centrifugally forces, pronounced more at the lowest and the highest rotation rates (see figure 4), does not change the trend. Associated to the centrifugally driven flow, the vortex $\omega_{\max} = (1/r)\{\partial^2\psi/\partial r^2 + \partial^2\psi/\partial z^2 - (1/r)\partial\psi/\partial r\}$ magnitude is affected by the Coriolis and thermocapillary forces.
The numerical results, with and without Marangoni flow, are plotted in figure 5. Increasing the rotation rate, $\omega_{\max}$ is lowered to a minimum at around $|\Omega_c| = 1.571\ rad/s$ (~15 rpm), and the raised sharply by further increase in Ω_c. Again, thermocapillary forces modify the curve, particularly in the lower range of rotation, but the general feature of the curve remains the same. For the GaAs melt parameterized in the model by so high $\mathrm{Ma}/\mathrm{Pr}\,\mathrm{Gr}^{1/2}$ as ~180, the result is unexpected.

According to the scaling analysis, in the interior of the melt $\psi_\sigma/\psi_\beta = 4(\mathrm{Ma}/\mathrm{Pr})^{1/3}/\xi^{1/2}Gr^{1/2}$, where ψ_σ and ψ_β are the magnitudes of Marangoni and buoyancy flow stream functions, respectively and ξ appears in $\Delta T_M = \xi\,\Delta T_{\max}$ [29]. The temperature at the point M_i was computed for the applied range of rotation and found to be $T_M = 9.5 \pm 1.4\ K$ leading to $\xi \sim 0.53$ and $\psi_\sigma/\psi_\beta \sim 1/10$.

It was found that the tilt angle, θ_ψ is directly related to the Ekman shear angle in its model-adopted form $\chi(r) = 4.746 \times 10^{-3}\pi^2\Omega_c(r_c^2 - r^2)$, simply by $\tan\theta_\psi = 1 - \tan\chi(r)$ at the point K ($r = r_c/2$, $z = \delta_E$) on the line E close to the crucible bottom. Herein, the angles are in degrees, Ω_c in rpm, $r_c = 7.50\ cm$, and $\delta_E = (\nu/|\Omega_c|)^{1/2}$ is ~1.0 mm for $\Omega_c = -5.0\ rpm$ as the Ekamn layer thickness. Increasing in Ω_c, the number of spiral arms $N_E = |\mathrm{Re}_c|/16\pi$ with separation $\Delta r = (1/4N_E)(r_c^2/r)$, increases. This can be readily verified that the line E separates apart the smaller spirals near the corner and the larger spirals near the axis of rotation, corresponding to the smaller and larger deformations of the flow volume element. Supposed that increasing the rotation rate intensifies the effect and referred to the simple relation between θ_ψ and $\chi(r)$, development of the spiral shearing flow might be assumed to explain the LSC rotation around the vortex vector $\boldsymbol{\omega}_{\max}$.

3.3. Flow modes in the GaAs melt rotating with its container

Referred to figure 3 (a-g)**,** it appears that between the LSC and the rotation axis, there is an ovidal shape small roll with $\psi/\psi_{\max} \sim 0.4$**.** The cell is located below the convex to melt part of the phase boundary and centered approximately on the line b crossing the inflection point I on the crystallization front. Emerged from the centrifugally driven cell, and circulating in the same direction as LSC, the intensity of this small convection found to be, in contrast to LSC, approximately independent of the rotation rate. Its shape, however, is modified by increasing Ω_c. for lower rotation rates, $|\Omega_c| < 7.5\ rpm$ and at the same shape, the thermal field exhibits an undulating structure in the melt leading to a radial non-uniformity of the thermal field close to the phase boundary. The effect is suppressed by further increase in the rotation rate ($|\Omega_c| > 7.5\ rpm$) due to the overstability known [20] as a distinctive feature of convection with rotation. This behavior implies that the Rayleigh-Benrad instability occurs at low rotation rates. In fact, when the buoyancy and Coriolis forces are comparable, $(\mathrm{Gr/Ta}) \sim 1$, the Coriolis force will prevent vertical convection against the conservation of angular momentum and the oscillations decrease close to the onset boundaries. Herein, the ratio $\mathrm{Gr/Ta}$ equals to unity when $|\Omega_c| = 8.78\ rpm$ as confirmed by simulations of the fields in figure 3(a-f).

For the imposed and calculated (at the point M_i) temperature differences $\Delta T_r = \Delta T_{\max}$ and $0.8 \le \Delta T_{m,i} \le 12.5\ K$, respectively, the flow modes in the GaAs melt rotating at different rates are represented in figure 6 as the two-parameter regime diagram. Note that $\partial T/\partial z \cong 4.2\ K/cm$ at the point M_i found to be close to the data given by Kaoi et al [30]. Therefore, the vertical temperature difference ΔT_z is close to $\Delta T_{m,i}$ in the model.

The knee-shaped curve of transition obtained from the experimental results [15] for mercury ($\mathrm{Pr} = 2.46 \times 10^{-2}$) shows that, at lower rotation rates the flow appears to be axisymmetric in the regime diagram. As mentioned before, the flow field is dominated by the Küppers-Lortz instability for $|\Omega_c| < 8.77\ rpm$. The enhancement of Coriolis forces complicates the flow pattern due to the baroclinic instability. Numerical results in figures 7(a) and 7(b) reveal that how the local temperature difference and velocity components at the mid-depth/mid-radius of the melt, namely at the point M_i in the interior, vary with rotation. For more realistic case in the model, that is when $\mathrm{Ma} \neq 0$, both $u_{m,i}$ and $T_{m,i}$ decrease considerably with Ω_c in the lower range of rotation $5 < |\Omega_c| < 10\ rpm$. Remarkably, the flow velocity $u_{m,i}$ is raised by a further increase in Ω_c up to a maximum at $\Omega_c = -12.5\ rpm$ and then lowered more sharply in higher range of rotation, $12.5 < |\Omega_c| < 15.0\ rpm$. Decreasing $T_{m,i}$ in the lower rotation range corresponds to higher value of the Rossby number Ro_T (due to larger $\Delta T_{m,i} = T_c - T_{m,i}$) and lower values of the Taylor number ($\mathrm{Ta} < 10^7$) in the regime diagram. By further increase in Ω_c , the onset of a baroclinic wave occurs at $\mathrm{Ro}_T = 2.06$ ($\Delta T = 18\ K$ and $\Omega_c = -7.2\ rpm$) corresponding to $\mathbf{Ta} = 1.417 \times 10^7$. For silicon melt, this critical Rossby number was 2.4 according to theoretical investigations [31]. The points which lie on the line II (see figure 6) stand for non-axisymmetric flow with regular wave [15]. At rotation rates $|\Omega_c| \geq 15\ rpm$ and for the imposed $\Delta T = \Delta T_{\max}$, the points located under the line II represent the stabilization of the flow at $\mathrm{Ro}_T \leq 0.476$ and $\mathrm{Ta} \geq 6.152 \times 10^7$. The transition is qualitatively similar to experimental data [32] in which it occurs at Ro_T number considerably lower than unity.

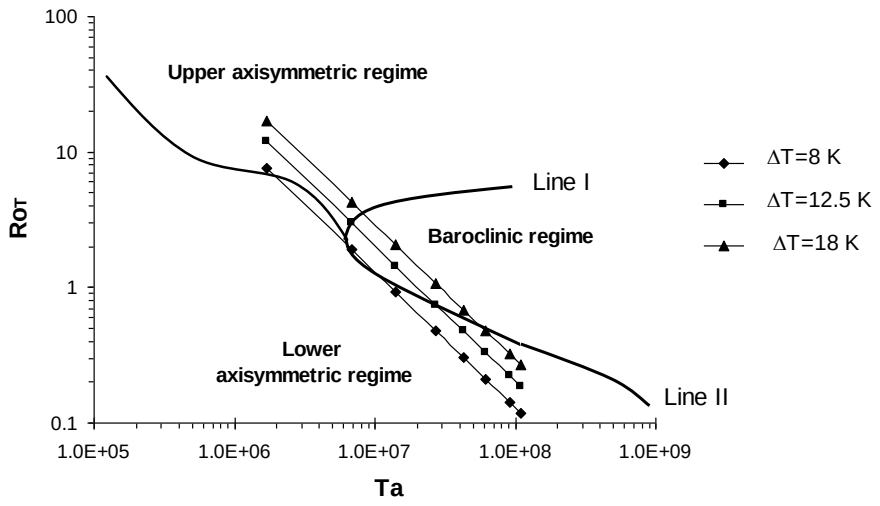

Figure 6: Flow modes at different rotation rates ($2.5 \leq \Omega_c \leq 20\ rpm$) for the imposed horizontal and vertical temperature differences $\Delta T_r = 18\ K$ and $8.0 \leq \Delta T_z \leq 12.5\ K$, respectively. The transition curve obtained from Fein-Pfeffer's experimental results [15]. The two lines stand for the upper and the lower boundaries for the occurrence of baroclinic instability.

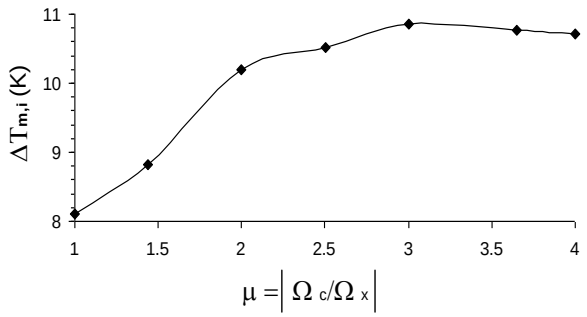

Figure 7(a): Rotational effect on temperature variation in the interior of the melt.

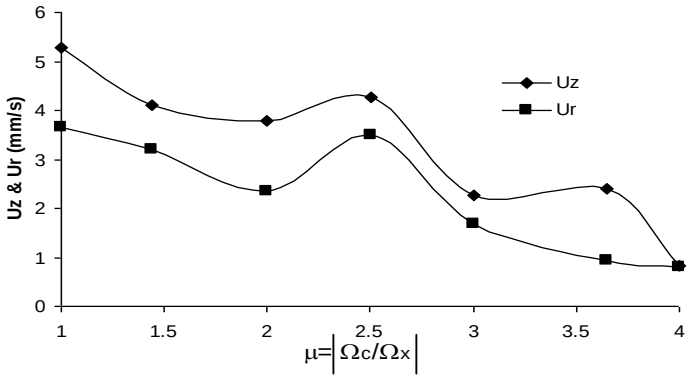

Figure 7(b): Rotational effect on the components of flow maximum velocity in the interior of the melt.

IV. CONCLUSION

The GaAs flow field structure and temperature distribution were described in the present model calculations. It was demonstrated that even perfectly axisymmetric geometries may exhibit flow instabilities. Simulations of the melt flow even at the lowest applied rotation rate $\Omega_c = -0.524\ rad/s$ revealed that buoyancy driven flow characterized by a unicellular meridional circulation is compressed by a strong centrifugally driven roll (LSC). Throughout the simulations, LSC appeared as the dominant flow in the multicell structure of the GaAs melt rotating with its container. In contrast to the large magnitude of $Ma/Pr\,Gr^{1/2}$, it was shown that the convective flow pattern does not depend strongly on the presence of thermocapillary forces. In fact, in the interior of the melt ψ_β/ψ_σ as the ratio between the buoyancy and thermocapillary forces largely exceeds the unity.

Increasing the rotation rate $0.524 < |\Omega_c| < 2.094\ rad/s$, the dominant cell (LSC) found to rotate around the vortex vector $\boldsymbol{\omega}_{\max}$ by an angle θ_ψ directly related to the Ekman shear angle. Decreasing the intensity of the cell, the Coriolis force enhancement suppresses the undulating structure of thermal field. The so-called overstability of the melt was broken by further in the rotation rate. The appearance of the baroclinic wave region in the flow regime diagram corresponds to the transition from axisymmeteric to non-axisymmetric flow. The transition found to be sensitive to the applied temperature difference and as ΔT increases, a regular wave gives way to an irregular wave. The onset of baroclinic wave found to occur at $Ro_T = 2.07$ when $\Delta T = 18\ K$. According to the experimental analysis [32] the transition is associated with significant increase in the amplitude of temperature fluctuation close to the phase boundary. As shown in the regime diagram, the baroclinic thermal wave disappears when the rotation-driven convection overcomes the buoyancy-driven convection.

The present model analysis may ensure axisymmetric flow and thermal fields in the melt characterized by $Ro_T \le 0.476$ and $Ta \ge 6.152 \times 10^7$. The results correspond to the rotation rate $|\Omega_c| \ge 1.571\ rad/s$ and $\mu = |\Omega_c/\Omega_x| \ge 3$, close to the parameters used in the industrial scale growth ($|\Omega_c| = 1.676\ rad/s$ and $\mu = 2.7$) of the GaAs crystals. Notable is that the vortex of the dominant circulation $\boldsymbol{\omega}_{\max}$ found to meet its minimum value at around $|\Omega_c| = 1.571\ rad/s$.

REFERENCES

[1.] M.R. Brozel, I.R. Grant, Growth of gallium arsenide, in: P. Capper (Ed.), Bulk Crystal Growth of Electronic, Optical and Opto-electronic Materials, John Wiley, UK, 2005, pp. 43-71.
[2.] J.B. Mullin, Progress in the melt growth of III-V compounds, J. Cryst. Growth 264 (2004) 578-592.
[3.] A. Yeckel, J. J. Derby, Computational simulations of the growth of crystals from the liquid, in: H.J. Scheel, T. Fukada (Eds.), Crystal Growth Technology, John Wiley, UK, 2003, pp.115-137.
[4.] V.I. Polezhaev, Modelling of hydrodynamics, heat and mass transfer processes on the basis of unsteady Navier-Stokes equations. Applications to the material sciences at earth and under microgravity, Comput. Methods Appl. Mech. Engrg. 115 (1994) 79-92.
[5.] T. Tsukada, M. Kobayashi, C.J. Jing, N. Imaishi, Numerical simulation of Cz crystal growth of oxides, FDMP 1 (2005) 45-62.
[6.] S. Gondet, T. Duffar, G. Jacob, N. Van der Bogart, F. Louchet, Thermal stress simulation and interface destabilisation in indium phosphide grown by LEC process, J. Cryst. Growth, 198/199 (1999) 129-134.
[7.] N. Miyazaki, H. Kutsukake, A. Kumamoto, Development of 3D dislocation density analysis code for annealing process of single crystal ingot, J. Cryst. Growth 243 (2002) 47-54.
[8.] M. Jurisch, St. Eichler, The development of LEC technology for GaAs single crystal growth from laboratory scale to mass production, in: Proceeding of the Czochralski Symposium, Torun/Kcynia, Poland, 2003.

[9.] D. Vizman, S. Eichler, J. Friedrich, G. Muller, Three-dimensional modeling of melt flow and interface shape in the industrial liquid-encapsulated Czochralski growth of GaAs, J. Cryst. Growth 266 (2004) 396-403.
[10.] K. Koai, Model-based thermal stress control of LEC GaAs bulk crystal growth, PhD thesis, Mechanical Engineering Department, MIT, Cambridge, MA (1990).
[11.] M. Shibata, T. Suzuki, S. Kuma, T. Inanda, LEC Growth of Large GaAs Crystals, J. Cryst. Growth 128 (1993) 439-443.
[12.] T.C. Chen, H.C. Wu, C. I. Weng, The effect of interface shape on anisotropic thermal stress of bulk single crystal during Czochralski growth, J. Cryst. Growth 173 (1997) 367-379.
[13.] S. Chandrasekhar, Hydrodynamics and Hydromagnetic Stability, Clarenden Press, Oxford, 1961.
[14.] P.C. Drazin, w.H. Reid, Hydrodynamic Stability, Cambridge Univ. Press, Cambridge, 1981.
[15.] J.S. Fein, R.L. Pfeffer, An experimental study of the effects of Prandtl number on thermal convection in a rotating, differentially heated cylindrical annulus of fluid, J. Fluid Mech. 75 (1976) 81-112.
[16.] J.R. Ristorcelli, J.L. Lumely, Second order turbulence simulation of Cz crystal growth melt, J. Cryst. Growth 129 (1993) 249-265.
[17.] K. Kakimoto, Flow instability during crystal growth from the melt, Prog. Cryst. Growth and Charat. 30 (1995) 191-215.
[18.] V.I. Polezhaev, O.A. Bessonov, N.V. Nikitin, S.A. Nikitin, Convective interaction and instabilities in GaAs Czochralski model, J. Cryst. Growth 230 (2001) 40-47.
[19.] F. Rosenberger, Fundamental of crystal growth I, Springer, Berlin, 1979.
[20.] E.L. Koschmieder, Benard Cells and Taylor Vortices, Cambridge Univ. Press, Cambridge, 1993.
[21.] J.R. Ristorcelli, J.L. Lumely, Instabilities, transition and turbulence in the Czochralski crystal melt, J. Cryst. Growth 116 (1992) 447-460.
[22.] A. Rubio, J.M. Lopez, F. Marques, Onset of Küppers-Lortz-like dynamics in finite rotating thermal convection, J. Fluid Mech. 644 (2010) 337-357.
[23.] Th. von Larcher, C. Egbers, Experiments on transitions of baroclinic waves in a differentially heated annulus, Nonlinear Processes in Geophys. 12 (2005) 1033-1041.
[24.] M. Li, W. Hu, N. Chen, D. Zhang, Z. Tang, Numerical analysis of LEC growth of GaAs with an axial magnetic field, Int. J. Heat Mass Transfer 45 (2002) 2843-2851.
[25.] V.I. Polezhaev, Modeling of Technologically Important Hydrodynamics and Heat/Mass Transfer Processes During Crystal Growth, in: H.J. Scheel, T. Fukuda (Eds.), Cryst. Growth Technology, John Wiley & Sons, West Sussex, 2003, pp. 155-186.
[26.] J.H. Ferziger, M. Perić, Computational Methods for Fluid Dynamics, 3rd Edition, Springer, Berlin, 2002.
[27.] S. Carra, S. Fogliani, M. Masi, L. Zanotti, C. Mucchino, C. Paorici, Melt-solid interface shape in LEC GaAs crystals: comparison between calculated and experimentally observed shapes, J. Cryst. Growth 166 (1996) 641-645.
[28.] G. Müller, A. Ostrogorsky, Convection in melt growth, in: D.T.J. Hurle (Ed.), Handbook of Crystal Growth, Basic Techniques, Vol. 2b, North Holland, 1994, pp. 710-820.
[29.] A.D.W. Jones, Scaling analysis of the flow of a low-Pr number Cz melt, J. Cryst. Growth 88 (1988) 465-476.
[30.] K. Kaoi, A. Seidl, H.-J. Leister, G. Muller, A. Kohler, Modeling of thermal fluid flow in the liquid encapsulated Czochraslki process and comparison with the experiment, J. Cryst. Growth 137 (1994) 41-47.
[31.] Y. Kishida, M. Tanaka, H. Esaka, Appearance of a baroclinic wave in Czochralski silicon melt, J. Cryst. Growth 130 (1993) 75-84.
[32.] Y.S. Lee, C.H. Chun, Transition from regular to irregular thermal wave by coupling of natural convection with rotating flow in Czochralski crystal growth, J. Cryst. Growth 197 (1999) 297-306.

Figure and table captions *should be 10-point boldface Helvetica (or a similar sans-serif font). Callouts should be 9-point non-boldface Helvetica. Initially capitalize only the first word of each figure caption and table title. Figures and tables must be numbered separately. For example: "Figure 1. Database contexts" , "Table 1. Input data". Figure captions are to be centered below the figures. Table titles are to be centered above the tables.*

ISSN (e): 2250 – 3005 || Volume, 05 || Issue, 07 || July – 2015 ||
International Journal of Computational Engineering Research (IJCER)

SEISMIC ANALYSIS OF R.C.C. AND STEEL SILOS

Krishna T. Kharjule[1], Minakshi B. Jagtap[2]
[1] PG student with the Department of Civil Engineering, Vidya Pratisthan's collage of Engineering, Baramati Pune
[2] Professor with the Department of Civil Engineering, Vidya Pratisthan's collage of Engineering, Baramati Pune

Abstract
Structures used for storing bulk solids are called bins, bunkers, silos, or tanks. There is no generally accepted definition for these terms, shallow structures containing coal, crushed stone, gravel, and similar materials are called bins or bunkers and tall structures containing materials such as grain, cement and wheat are usually called silos. Elevated silos generally consist of a conical roof, a cylindrical shell and a conical hopper and they could be elevated and supported by frames or reinforced concrete columns. Circular silos (both steel and reinforced concrete) are used to store material in various industries like cement plants (clinkers), power plants(raw coal), oil and gas industry(sulfur pellets) etc.Elevated steel and reinforced concrete circular silo for storage show performance in earthquake reinforced concrete silo stability increases by using shear wall but loss of steel silo in earthquake stability increases using steel panel on opposite side Displacement of structure decreases in case of shear wall panel and stiffness increases.

Keywords: *Elevated* silos, response spectrum analysis, shear wall, steel plate, time history analysis**.**

I. INTRODUCTION

Silos are an inclusive term of all structures for the storage of bulk solids common use, may be ground-supported or elevated. Typical elevated silos generally consist of a conical roof, a cylindrical shell and a conical hopper and they could be elevated and supported by frames or reinforced concrete columns or on discrete supports. Silos are lifeline structures and strategically very important, since they have vital use in industries. Silos are special structures subjected to many different unconventional loading conditions, which result in unusual failure modes. Silos are cantilever structures with the material stacked up very high vertically. The walls of different type of silos are subject to earthquake loads from the stored mass, and these may substantially exceed the pressures from filling and discharge. The elevated silos response is highly influenced by the earthquake characteristics and is depending on the height to diameter ratio. In the earthquake analysis of such structures is to consider the silo and its content as a lumped mass and seismic effect of this mass is considered in design of the supporting frame only. Failure of a silo can be devastating as it can result in loss of the container, contamination of the material it contains, loss of material, replacement costs, environmental damage, and possible injury or loss of life. Silos and bins fail with a frequency which is much higher than almost any other industrial equipment. Sometimes the failure only involves distortion or deformation which, while unsightly, does not pose a safety or operational hazard.

II. MODELING

Four models of the present work were used to analyze elevated silos R.C.C. silos with and without shear wall and steel silos with and without shear wall panel use M20 and Fe 500.

Table 1 Dimension of silos

Height of cylindrical portion	18m
Height of conical portion	2.5m
Height of column	5m
Internal diameter	5.5m
Central opening	0.5m
Diameter of column	500mm
Thickness of shell	300mm
Size of beam	300X600mm

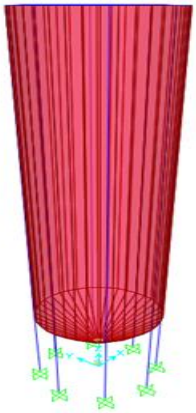

Fig.1 R.C.C. Silo without shear wall

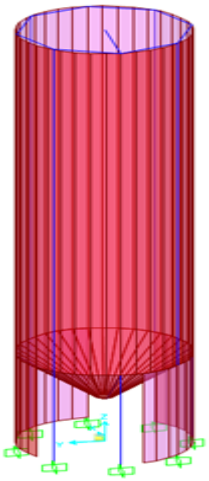

Fig.2 R.C.C. Silo with shear wall

III. RESULTS AND DISSCUTION

In R.C.C. Silo with maximum displacement in case of without shear wall but provide shear wall on the opposite side displacement due to earthquake loading is decrease. Wall thickness of shear wall is same as thickness of cylindrical portion. In case of Steel silos steel plate is provided as function of shear wall displacement of steel silo is decrease by using steel plate and stability of structure is increases. Time period of structure is less of both cases R.C.C. and steel silos by using shear wall.

Table 2 Top displacement in (mm)

R.C.C. Silo without shear wall	R.C.C. Silo with shear wall
U1=11.6742	U1=6.9956
U2=0.0015	U2=0.6928
U3=0.0927	U3=0.1468
Steel Silo without shear wall	Steel Silo with shear wall
U1=19.4412	U1=3.5691
U2=0.0006	U2=0.286
U3=0.2946	U3=0.5068

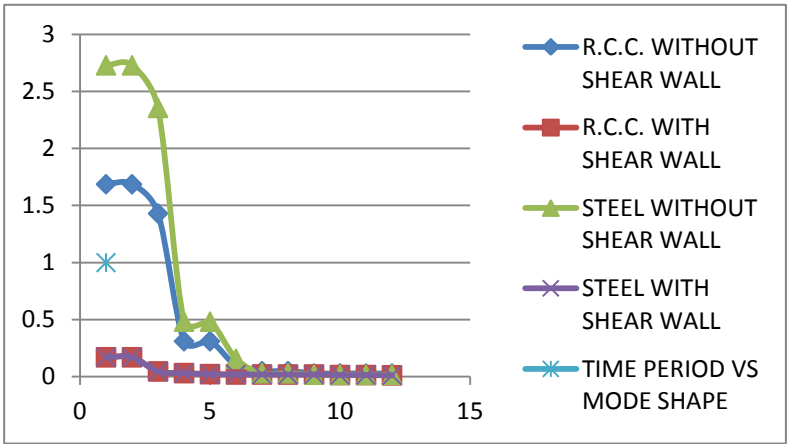

Graph 1 Time period Vs Mode shape

Acceleration results for full loaded condition (Acceleration Vs Time)

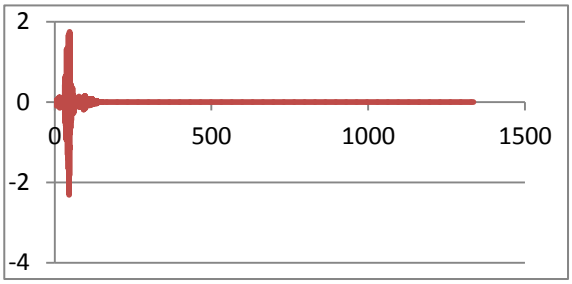

Graph 2 R.C.C. Silo with shear wall

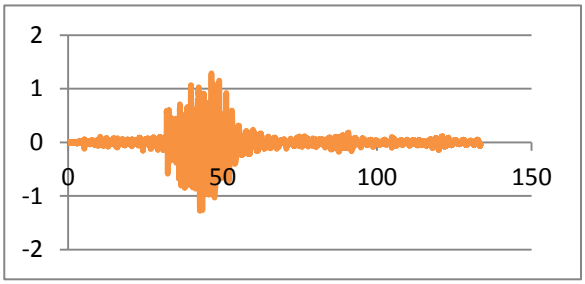

R.C.C. Silo without shear wall

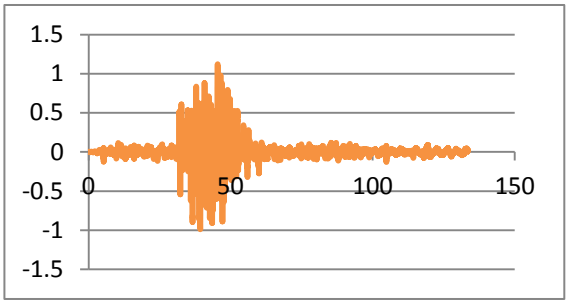

Graph 3 Steel Silo with shear wall

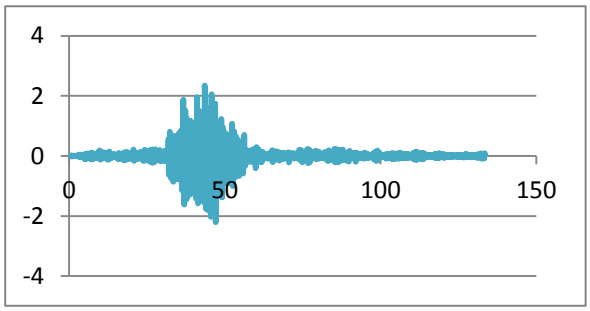

Steel Silo without shear wall

Base Shear results for full loaded condition (Base Shear Vs Time)

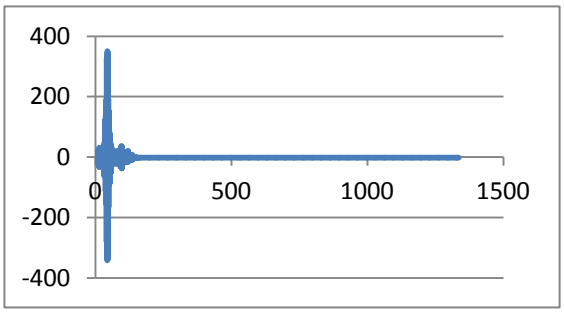

Graph 4 R.C.C. Silo with shear wall

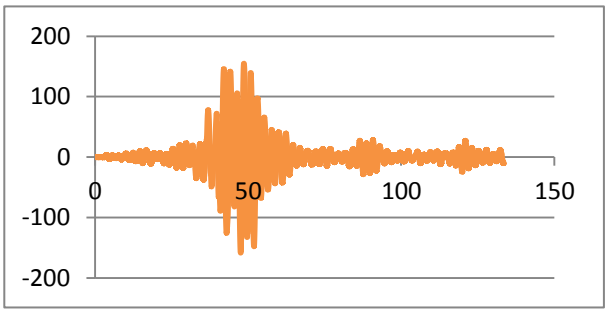

R.C.C. Silo without shear wall

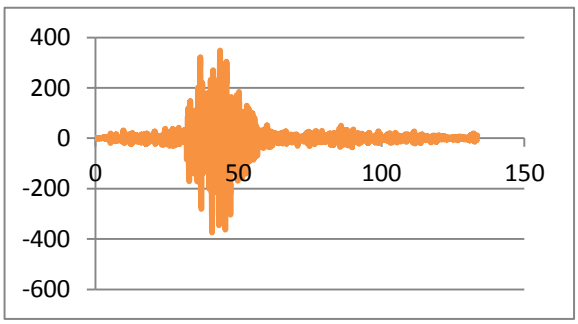

Graph 5 Steel Silo with shear wall

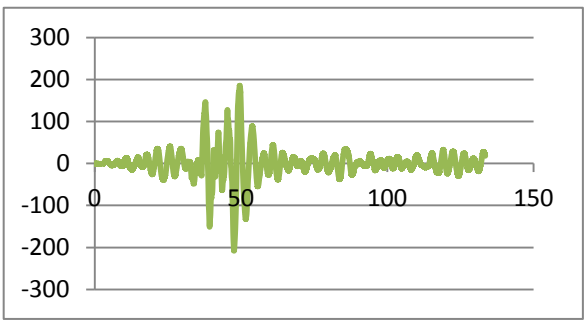

Steel Silo without shear wall

IV. CONCLUSION

R.C.C. Silos and steel silos in RSM method with shear wall displacement of structure is reduce compare to without shear wall. Due to using shear wall time period of structure is reduces. In Time history analysis acceleration of silo structure is decreases and base shear is increases in both cases R.C.C. Silos and steel silos with shear wall.

V. REFERENCES

[1] Hamdy H.A. Abdel-Rahim1 'Response the Cylindrical Elevated Wheat Storage Silos to Seismic Loading" ISSN (e): 2250-3021, ISSN (p): 2278-8719 Vol. 04, Issue 01 (January. 2014), ||V6|| PP 42-55.
[2] F. nateghia, M. yakhchalian 'Seismic Behavior of Reinforced Concrete Silos Considering Granular Material-Structure Interaction" Procedia Engineering 14 (2011) 3050–3058.
[3] Ashwini Bidari, K.N.Vishwanath 'Analysis of Seismic and Wind Effect on Steel Silo Supporting Structures" Vol.2, No.9, September 2014 E-ISSN: 2321-9637
[4] Sivabala. P, Elangovan. G, Kameshwari. B 'Effect of shear wall panels on the dynamic response of a silo" Volume 1, No 4, 2011.
[5] Indrajit chowdhury and Raj tilak 'Dynamic pressure on circular silos under seismic force December 17-19, 2010.
[6] Indrajit chowdhury and Jitendra pratap singh 'Dynamic response of rectangular bunker walls considering earthquake force January 4 to 6 2012 paper no. CNP008.
[7] Mueller, P. Knoedel, B. Koelle 'Critical Filling Levels of Silos and Bunkers in Seismic Design" 15 WCEE LISBOA 2012.
[8] Er. Amit Bijon Dutta 'Study of Types of Failures in Silos" Volume: 2 | Issue: 11 | Nov 2013 • ISSN No 2277 – 8160.

ISSN (e): 2250 – 3005 || Volume, 05 || Issue, 07 || July – 2015 ||
International Journal of Computational Engineering Research (IJCER)

Social Media Applications for Project Management

Alina Mannanova
North-West Institute of Management – branch of Russian Presidential Academy of National Economy and Public Administration. V.O. Srednij pr. 57, 199178 St. Petersburg

Abstract:
Project communication and collaboration is a crucial activity that makes or breaks a project. Excellent technical skills and intuition may be insufficient to drive performance if not accompanied by appropriate levels of interpersonal interaction within project groups. Evidently that Global participation platforms and social networks like Facebook, LinkedIn and others and a mass of local blogs and web communities are an important source for next generation of project managers. How these new technologies will impact organizations, however, is not entirely clear. Therefore, it represents an important field for information systems research. This paper presents a survey study of the intrusion of social media in project management. We investigate some basic questions such as the possibilities, dangers, and limits (e.g. legal or ethical) of using social media services in project management. Also we analyzed the existed approaches that can serve as a start point for the successful and efficient implementation of such services. Ours results indicate that social media analysis can serve as an improvement tool for project management to reduce the product development time and associated cost through the implementation of social network analysis

Keywords: Social media, social media network, project management, blog, wiki, information technology

I. INTRODUCTION

Historically, the industry has focused extensively on optimizing the project management *(PM).* In this focus, organizations have emphasized the ability to develop the optimum plan, allocate resources efficiently, and utilize control functions to ensure that the project stays on schedule and within budget. This used to be effective however nowadays this engineering focus has reached the point of diminishing results. Specifically, the engineering approach to PM has neglected to recognize the importance of the participants to the success of the overall project.

Simultaneously, over time, social networks (*SN*) have evolved and this evolution has kept pace with the growing needs of businesses and their needs. Accordingly, social media applications (*SMA*) are increasingly widespread in modern societies. INTERNET use and mobile access to information, SN, entertainment and services are and will be subject to rapid growth and create an essential source for so called “social media analytics”, which allow to monitor and analyze user generated contents for different purposes systematically. Given this prominence social media (*SM*) have reached in different fields, we identify a crucial importance to promote the application of SM services for effective PM in different domain as well as positive product development process (*PDP*).

Based on current possibilities and evolving practices of SM usage as a means of community participation, this paper develops ideas for a future use of SM in PDP as a tool for PM. The opportunities, which are meant to be identified, will be weighed up against potential risks and weaknesses of the incorporation SMA in PM.

II. WHAT IS SOCIAL NETWORK ANALYSIS AND SOCIAL MEDIA

Writing in 1857, Karl Marx (1939: 176) puts it nicely: "Society does not consist of individuals, but expresses the sum of interrelations in which individuals stand with respect to one another". Social network analysis (*SNA*) has appeared in the social sciences for nearly a century (Borgatti et al. 2009). A network is a set of nodes interrelated by dyadic ties. The nodes, or actors, can consist of any kind of entity, from individuals to collectives (e.g., organizations, countries).

SNA is the mapping and measuring the relationships and flow among the information entities [10], the technique used to study the relationships among actors, such as people or organizations. SM can be defined as a digital media or technology allowing their users to share information and other contents individually or within a community, a tool that link individuals by providing a common platform for discussion in one centralized and easily accessible place. Such tools also create opportunities to move beyond information sharing and venting personal frustrations to real action by motivating, inspiring and organizing users [25]. It is difficult to clarify what is technologically distinctive about SM technologies. The broad term has been used to apply a variety of technologies, including wikis, blogs, micro-blogs, SN-ing sites, virtual worlds, video-sharing sites and many others [13]. Researchers updated a widely used definition of SN-ing sites to highlight four features shared by many SM technologies: *digital profile, relational ties, search and privacy, network transparency* [12]. To sum up let us point out that *SM in PM is:*

- a medium for interactive social interaction using communication technologies where INTERNET is a platform;
- a community based, interactive content, user generated content;
- a form of social software which fosters engagement and interaction [23];
- a community and collaboration based technology that is merely a facilitator tool.

III. PROJECT MANAGEMENT 2.0 AND SOCIAL PROJECT MANAGEMENT

In response to PM challenges, project teams have turned to technology to attempt to streamline collaboration. The most visible recent development in technology-enabled project collaboration is the movement called "*Project Management 2.0*" (PM 2.0) which has been defined in a number of ways, but the basic definition of the PM 2.0 is the use of Web 2.0[*] technologies to enable project teams to better share information, increase collaboration and to empower teams to get things done.

However, it is difficult to define what makes a particular technology a PM 2.0 technology. The most common example used is the Project Wiki and blogs where all of the team members can update as necessary any project information (the tasks required, the status of tasks, project roles and responsibilities, etc.). INTERNET search engines and Wi-Fi[**] are general-purpose technologies as it is hard to define when their use is for PM.

The researchers of the Trilog Group Whitepaper [27] advocate that Social project management (SPM) goes far beyond PM 2.0 by recognizing that project teams are only part of the project community[***] and that a broader project community exists, both formal and informal, and that the engagement of that community is the key to building trust and knowledge. SPM makes it possible the engagement of the full SN of the project community, in order to achieve the project's goals. Rather than focusing merely on the needs of each project team individually, SPM strives to focus on the needs of an organization, by engaging the largest number of appropriate SN ties in accomplishing the goals of all the projects of an organization.

Characteristics of SPM

- Engaged - deeply connecting people, including customers, employees, and partners, to be involved in productive, efficient ways;
- Transparent - removing boundaries to information, experts and assets, helping people align every action to drive business results;
- Nimble - speeding up business with information and insight to anticipate and address evolving opportunities.

SPM builds on the gains made by PM 2.0 by enabling teams to bring their core PM process online. Then, by applying the SN-ing (i.e. Facebook) paradigm to the core business process, SPM Software makes the project process visible to everyone, both inside and outside the team. Without sacrificing traditional PM rigor, SPM gives the internal and external project community visibility into the events of the project, as they happen, allowing teams to achieve transparency as to project progress and status, and to enable smarter and more efficient collaboration. Further, using the "re-tweet" paradigm, project teams can publish issues, needs, and questions to the wider corporate (and external) SN, allowing for anyone who is interested to engage socially with the team to assist in accomplishing the project and organization's goals.

[*] World Wide Web sites that use technology beyond the static pages. A Web 2.0 site allow users to interact and collaborate with each other in a SM dialogue as creators of user-generated content in a virtual community.

[**] Is a local area wireless technology that allows an electronic device to participate in computer networking using 2.4 GHz UHF and 5 GHz SHF ISM radio bands.

[***] Project Community – the entire social network related to a project, including the team, stakeholders, management, and other interested parties.

SM has not only become an integral part of people's personal lives but also embedded itself into various business processes (Fig. 1): it is playing a critical role in the digital marketing strategy of a business, is an instrumental in improving the customer engagement, is also used to astute project managers as a part of their management strategy.

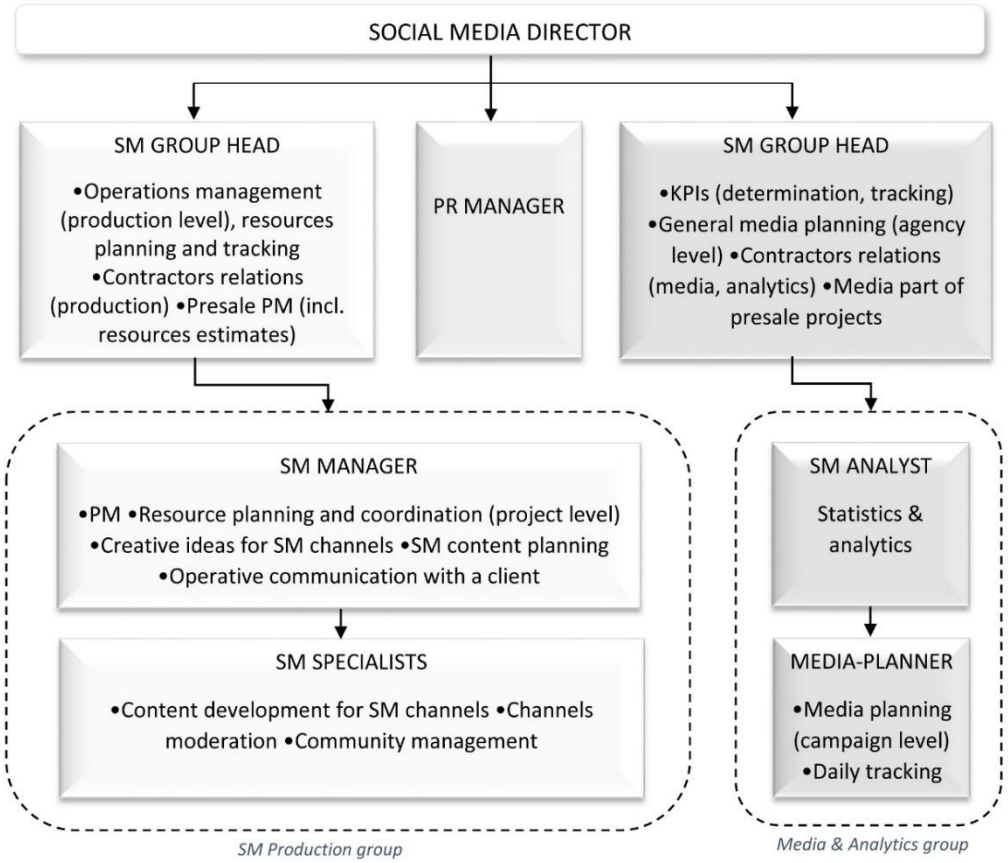

Fig. 1. A business model with integrated social media

These so-called SM-monitoring and analytics tools (e.g. commercial software tools[*]) are mainly developed for companies and organizations to gather information about their product placement and general business monitoring, the analysis and identification of new trends, as well as for their broader social marketing campaigns.

IV. PROS AND CONS

Traditional PM practices create defined and hierarchical communications paths. SPM recognizes that while these traditional communication and collaboration channels may reduce information and communication overload, they are too slow, filter out important information, and do not allow the right information to get to the right person.

There is a huge amount of PM software for the enterprise. Even so the essence of great PM is ensuring sustained useful interactions between the team, away from the software [1]. SM ensures communication within the team and between the project stakeholders. The idea behind incorporating SM into a PM process is to improve collaboration and create a more conducive environment (Fig.2) wherein problems are solved faster.

[*] Such as Opinion Tracker, Simplify360, Radian6, BrandsEye, Brandwatch Tool and many others (cf. Goldbach Interactive Social Media Monitoring Tool Report 2012: www.goldbachinteractive.com/aktuell/fachartikel/socialmedia-monitoring-tool-report-2012)

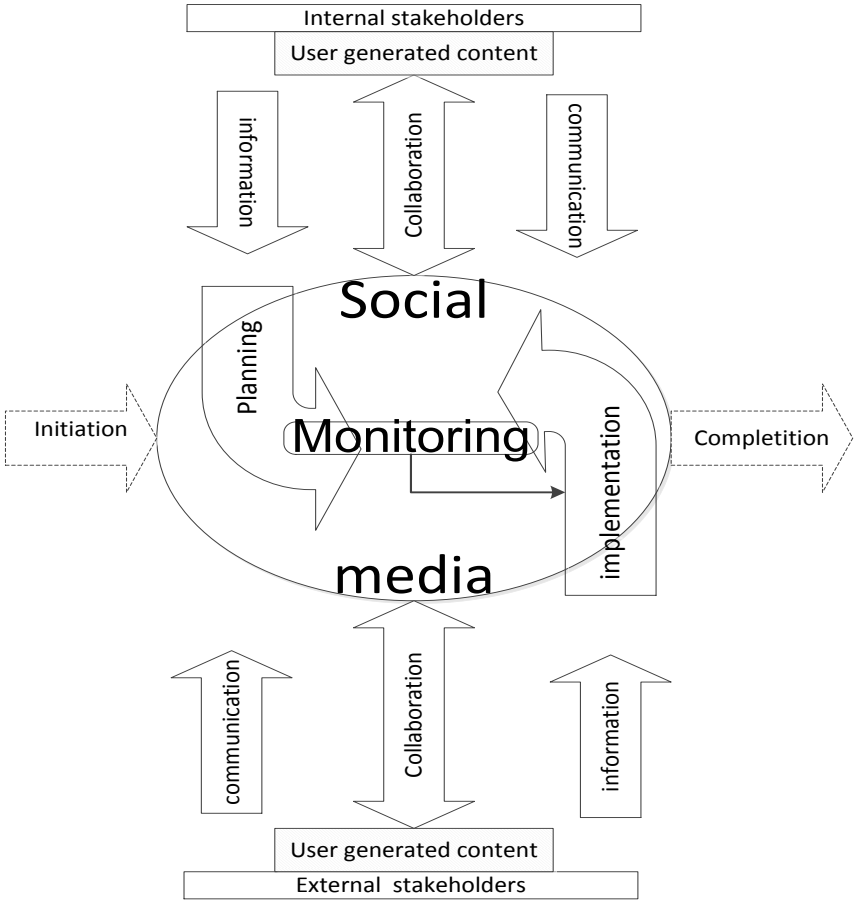

Fig. 2. Environment of social media for PM

Recently, project team members worked mostly in the same physical space, using PM applications on personal computers (exchange files on floppies, cd or flesh -devices) with weekly team meetings and senior management monthly information updates. Nowadays, project team workers do not depend on the physical space attendance and on the common working hours (eight-to-five). Senior managers have unlimited access to needed project information. Hence, the information exchange between the team members and stakeholders serves as the root source of continued competitive advantage [27].

Using social concepts to improve team communication is an exciting prospect, however, in the research by Rohan Ayyar pros and cons of implementing social into PM strategy are denoted [1]. Contrary to the declaration that merging SM with PM is a challenge, the author previses from using SMN since a SN's privacy features will hardly ensure data safety toward social integration in PM and as a result, it can become one of the bedrocks of a results-driven PM process. He concludes that SN should not be seen as an alternative to PM software, but a means of enhancing the channels of interaction that improve coordination between stakeholders of the project.

The use of Web 2.0 technologies to enhance project collaboration and coordination, assisted greatly in enabling teams, especially virtual teams, to collaborate and share information. However, these tools, such as wikis, blogs, online file sharing, while enabling participation and automation, do not assist the PM-er in the management of the core PM process, and in many ways make his work more difficult [26].

One reason why most organizations are hesitating to incorporate SM in their traditional communication strategy is that the mono-directional flow of information evolves into a multi-directional flow where the population can not only publicly respond to the news-issuing organization, but where individuals can communicate with each other without the organization being able to act as a regulating force [17]. SPM recognizes that the members of the project community need constant access to certain key information: project goal, set of tasks, the team members' skills and knowledge, required to complete a task, role assigned to each task, changes in the environment, that affect the team or the deliverable, specified source to get needed information and assistance. Having access to the information listed above is every project team's goal, however it is difficult to achieve in practice as the ability to access and search content through various applications raises questions about the necessity to protect content from others' access. Hence, privacy has become a crucial issue as the use and adoption of SM has grown [8].

Another issue of SM incorporation in PM lays in the existed between groups negative ties which have been presented by Everett and ABorgatti in *negative clique concept* [11]. Thus, we consider this concept crucial for PM that involve using negative cliques to guide interventions.

Additionally, user low technology literacy and lack of clear process are the common barriers of SM use in PM according to Joseph Guarino [9].

The researchers underline several key aspects of SMA usage:

- *Legal aspect* - it is data protection and privacy issues [11];
- *Ethical challenges* - is referring to awareness raising measures of all stakeholders of an SMA tool, notably of the end users [16];
- *Cultural aspects* – languages, written dialects, communication habits between men and women - which we consider as important management reality in nowadays Global economy.

McKinsey estimates that the economic impact of SM on business could exceed $1 trillion, most of which is gained from more efficient communication and collaboration within and across organizations [5].

Versus to Rohan Ayyar there is an assumption for the incorporating SMN into enterprise life that employees activity in SM within their personal time as well as at work based on SM leaders' actions:

- get vital snippets of information out to audiences fast (Twitter);
- naturally build groups with common interests and synergies (Facebook, Google+);
- spontaneously create space to exchange ideas and opinions (Meatballwiki);
- make information easy to assimilate (YouTube, Vimeo);
- attract interest and support for suggested projects (Kickstarter, Indiegogo).

Note on PM benefits from the use of SMN:

- project visibility and engagement with management and stakeholders;
- shared knowledge and ideas;
- improved organization and deployment of project teams, with more flexibility and productivity;
- faster, more effective collaboration yielding better decisions and higher quality output.

Obviously, the major reason why SM is now so important in successful project team is that it corresponds point by point to today's PM needs.

V. CONCLUSION

Social media is not a remedy for all problems that project management is confronted with. Therefore, they need to be seen as an addition to the traditional information and communication channels, not as a substitution. Given the fact that the INTERNET and mobile handheld devices are constantly pushing towards omnipresence, the incorporation of new media as an additional channel is only a matter of time, though their use will vary according to available resources, organization types, and other contextual factors (e.c. - cultural or legal background). We would also to note:

I. Source to high performance is the recognition by the team that the success of the team is of primary importance and that this success is based on the individuals openly exchanging knowledge for the benefit of the solution. The relationship between knowledge exchange and trust among the members of the team is crucial.

II. Different social networks have different working models[*]. Social strategy is specific to different organization according to the business objectives, challenges and corporate culture. Exclusively, the appropriate network with the right kind of model should be integrated within the existing communications architecture of the project management process to promote the professional interaction dynamics within project management team.

III. Social media and Web 2.0 applications have not only become an integral part of everyday life but also create new possibilities for the advancement of project management by the strategic collection and exploitation of information, communication and interaction between stakeholders of a project and team members. The use of Social media changes business models (e.g. outsourcing) as the technology options are abundant and cost effective. A Social project management is not just a project management that uses a Facebook page and a Twitter handle, it is - one that embraces and cultivates a spirit of collaboration and community throughout its organization both internally and externally.

IV. As outlined in this paper, the sanctity of a project can be undermined if the inflow, interpretation and outflow of project information is not properly controlled and managed. Thus, Social media policy

[*] While Twitter is founded on a micro-messaging model, Facebook is driven by shares, where content is distributed by users, LinkedIn is configured for professionals with its features wherein the connections take place in a formal environment.

should be followed up by each organization beginning with the establishing a guidelines, much like an Acceptable Use Policy sets of use, which must be concise and clear that explain a clear focus and purpose, IP** (Copyright and Trademarks, etc.), dealing with confidential and proprietary info, security issues.

The social network model for project management outlines an innovative and transformative approach to enhancing project team performance. The historic approach of emphasizing a continuing refinement of tasks as a basis for achieving high performance teams is not a viable approach to achieving significant performance improvement in projects. Rather, it is time to recognize the key role of individuals within project networks, including the communication and trust that is the basis for achieving high performance results. The social network model addresses fundamental research questions in this domain through the integration of social science and engineering concepts.

SM is not a technology, it is a culture, created, supported and enabled by various technologies and applications that are constantly growing and changing in which people think, act, and communicate in a completely different way. The social networks model demonstrates that new technology combined with a greater understanding of project networks and interdependencies provides a foundation for achieving high performance outcomes.

REFERENCES

[1]. Ayyar, R. (2014). Merging Social with Project Management: What are the Benefits?
[2]. Borgatti, S. P., Brass, D. J., Halgin, D. S. (2014). Social Network Research: Confusions, Criticisms, and Controversies. http://www.steveborgatti.com/research/publications
[3]. Borgatti, S. P., Foster, P. (2003). The network paradigm in organizational research: A review and typology. Journal of Management. 29(6): 991-1013.
[4]. Chinowsky, P., Diekmann, J., Galotti, V. (2008). Social Network Model of Construction. Journal of Construction Engineering and Management. ASCE.
[5]. Choi AL, Sun G, Zhang Y, Grandjean P. (2012). Developmental fluoride neurotoxicity: a systematic review and meta-analysis. Environ Health Perspect. 120:1362–1368.
[6]. Everett, M. G., Borgatti, S. P. (2014). Networks Containing Negative Ties. Social Networks 38:111–120. http://www.steveborgatti.com/research/publications
[7]. Gerhard G. van de Bunt, Rafael P. M. Wittek, Maurits C. de Klepper. (2005). The Evolution of Intra-Organizational Trust Networks. The Case of a German Paper Factory: An Empirical Test of Six Trust Mechanisms. Vol. 20(3): 339–369.
[8]. Gross, R., Acquisti, A. (2005). Information revelation and privacy in online social networks (the Facebook case). In *ACM Workshop on Privacy in the Electronic Society*. Retrieved December 18, 2008, from http://www.heinz.cmu.edu/~acquisti//facebook-gross-acquisti.pdf
[9]. Guarino, J. (2000/2003). Social Media for Project Managers.
[10]. Hanneman, R. A., Riddle, M. (2005). Introduction to Social Network Methods. University of California.
[11]. Johansson, F., Brynielsson, J., Quijan, M., N. (2012). Estimating citizen alertness in crises using social media monitoring and analysis. IEEE. 189-196. http://foi.se/Global/Our_knowledge/Decision_support_system_and_information_fusion/FOI-S--4091--SE.pdf
[12]. Kane, G. C., Labianka, M. A. G., Borgatti S.P. (2013-2014). What's Different About Social Media Networks? A Framework and Research Agenda.
[13]. Kaplan, A. M., Haenlein, M. (2010). Users of the world, unite! The challenges and opportunities of Social Media. Business Horizons. 53, 59-68 http://www.elsevier.com/locate/bushor
[14]. Kilduff, M., & Brass, D. J. 2010. Organizational social network research: Core ideas and key debates.Academy of Management Annals, 4: 317-357.
[15]. Kilduff, M., & Brass, D. J. 2010. Job design: a social network perspective. Journal of Organizational Behavior, 31: 309–318.
[16]. Krieger, B., Grubmüller, V. (2012). D 2.6. Legal, Cultural, and Ethical Aspects Report. UniteEurope (Deliverable). Retrieved December 18, 2012, from http://www.uniteeurope.org/images/deliverables/UniteEurope_D2.6.pdf
[17]. Laad, G., Lewis, G. (2012). Roles of Social Media in Crisis Communication. http://www.geraldlewis.com/publications/Role_of_Social_Media_in_Crisis_Communication_Jan_2012_Gitanjali_Laad.pdf
[18]. Latham, S. (2008). Spur Digital. Measuring Value from Social Media.
[19]. Mehra, A., Borgatti, S. P., Brass, D., Labianca, G. In Press. "The Social Network Perspective". In Stanley D. Brunn (Ed.) Engineering Earth: The Impacts of Megaengineering Projects. Dordrecht, The Netherlands: Springer Science+Business Media
[20]. Monge, P. R., & Contractor, N. S. (2003). Theories of communication networks. New York: Oxford University Press.
[21]. Moreno, J. L. (1934). Who Shall Survive: A New Approach to the Problem of Human Interrelations. 466.
[22]. Neal, R. (1997). Markov chain Monte Carlo methods based on "slicing" the density function. Technical Report No. 9722. Department of Statistics, University of Toronto.
[23]. Nielsen Social Media Report Q3 (2011). Social Software
[24]. O'Reilly, T. (2005). What Is Web 2.0. Design Patterns and Business Models for the Next Generation of Software. http://www.oreilly.com/pub/a/web2/archive/what-is-web-20
[25]. Rainer, K., Grubmüller, V., Pejic, I., Leitner, P. (2013). Social Media Applications in Crisis Interaction. Systems. Connecting Matter, Life, Culture and Technology. Volume 1. Issue 1.
[26]. Trilog Group Whitepaper (2012). Social Project Management: Engaging the Social Network to Deliver Project Success.
[27]. Why Social Networkers Now Rule Project Management? http://www.business2community.com/brandviews/getapp/social-networkers-now-rule-project-management

** IP (internet protocol) - standard which regulates computer connections on networks that make up the Internet (Computers)

ISSN (e): 2250 – 3005 || Volume, 05 || Issue, 07 || July – 2015 ||
International Journal of Computational Engineering Research (IJCER)

Effects of Temperature Dependent Viscosity and Thermal Conductivity in a Mixed Convection Boundary Layer Flow of a Micropolar Fluid towards a Heated Shrinking Sheet in presence of Magnetic Field

Smita Sahu[1] , P. K. Mahanta[2]
[1]Department of Mathematics, Dibru College, Dibrugarh-786601, Assam, India
[2]Department of Mathematics, Namrup College, Dibrugarh-786623, Assam, India

Abstract:
Effects of temperature dependent viscosity and thermal conductivity in a mixed convection boundary layer flow of a micropolar fluid towards a heated shrinking sheet in presence of magnetic field along with stagnation flow have been studied in the present work. The boundary layer equations are transformed into ordinary differential equations using similarity transformations. The effects of variable viscosity, variable thermal conductivity and the parameters involved in the study on the velocity, micro-rotation and temperature distribution profiles are investigated by solving the governing transformed ordinary differential equations with the help of Runge-Kutta 4th order method with shooting technique. The numerical results are shown graphically and discussed in detail.

Keywords: Heat transfer, Magnetic field, Micro polar fluid, Shrinking sheet, Stagnation flow,Thermal conductivity, Variable viscosity.

I. Introduction

The problems of flow and heat transfer in the boundary layers of a continuous stretching/shrinking surface have attracted considerable attention of researchers due to their numerous applications in industrial manufacturing processes. Some of the applications are extraction of polymer sheets, paper production, hot rolling and glass-fiber production. Eringen [1] formulated the micropolar fluid theory as an extension of the Navier- Stokes model of classical hydrodynamics to facilitate the description of the fluids with complex molecules .The micropolar fluids are generally defined as isotropic, polar fluids in which deformation of molecules is neglected. Physically, a micropolar model can represent fluids whose molecules can rotate independently of the fluid stream flow and its local vortices. Micro polar fluids have important applications in colloidal fluids flow, blood flows, liquid crystals, lubricants and flow in capillaries, heat and mass exchangers etc.

Stagnation point flows have also applications in blood flow problems, the aerodynamics extrusion of plastic sheets, boundary-layer along material handling conveyers, the cooling of an infinite metallic plate in a cooling bath, and textile and paper industries. Flows over the tips of rockets, aircrafts, submarines and oil ships are some instances of stagnation flow applications[2]. Hiemenz [3] started the study of stagnation flow problem and reduced the Navier-Stokes equations for the forced convection problem to an ordinary differential equation of third order by using similarity transformation. Chamkha [4] solved the problem of the laminar steady viscous flows near a stagnation point with heat generation/absorbing. The steady two dimensional point flow of a power law fluid over a stretched surface was studied by Mahapatra and Gupta [5]. The numerical solution of unsteady boundary-layer flow of an incompressible viscous fluid in the stagnation point region over a stretching sheet was presented by Nazar*et.al* [6] (using Keller box method). The problem of steady two dimensional laminar MHD mixed convection stagnation point flow with mass transfer over a heated permeable surface was examined by Abdelkhalek [7]. Two dimensional steady incompressible mixed convection non orthogonal stagnation flow towards a heated or cooled stretching vertical plate was considered by Yian *et.al* [8]. The solution of hydro magnetic steady laminar two dimensional stagnation flow of a viscous incompressible electrically conducting fluid of variable thermal conductivity over a stretching sheet was obtained by Sharma and Shing [9] using shooting method. Effect of viscous dissipation on heat transfer in a non-Newtonian liquid film over an unsteady stretching sheet was investigated by Chen [10]. Heat transfer over a stretching surface with uniform or variable heat flux in micropolar fluids was studied by Ishak *et. Al* [11].

Mahanta *et .al.*[12] discussed the effects of radiation of flow of second grade fluid over a stretching sheet through porous medium with temperature dependent viscosity and thermal conductivity. A numerical study of steady incompressible micro polar fluid in a two dimensional stagnation point flow towards a stretching sheet was investigated by Nazar *et.al* [13]. Chang [14] presented the solution of flow and heat transfer characteristic of mixed convection in a micropolar fluid along a vertical flat plate with conduction effects. Ishak *et.al* [15] studied steady stagnation flow towards a vertical surface immersed in a micropolar fluid. Rashidi et.al [16] investigated the mixed convection boundary-layer flow of a micropolar fluid towards a heated shrinking sheet.

In the above literatures, in most of the studies, the viscosity and the thermal conductivity of the ambient fluid were assumed to be constant. When the effects of temperature dependent viscosity and thermal conductivity are taken into account, the flow characteristics are significantly changed compared to the constant property case. In this paper, an attempt has been made in this study to find the effects of temperature dependent viscosity and thermal conductivity on a mixed convection two dimensional stagnation point flow and heat transfer of a steady viscous incompressible micropolar fluid towards a heated shrinking sheet in presence of magnetic field with viscous dissipation. Viscosity and thermal conductivity are assumed to be inverse linear functions of temperature.

II. Formulation of the Problem:

We consider two dimensional stagnation point flow of a micro polar fluid impinging normally on a heated shrinking sheet at a fixed flat plat coinciding with the plane $y = 0$. The flow is assumed to be laminar, steady, viscous and incompressible and except the fluid viscosity and thermal conductivity all the fluid properties are assumed to be constant. Also a magnetic field of constant intensity is assumed to be applied normal to the surface and the electrical conductivity of the fluid is assumed to be small so that the induced magnetic field can be neglected in comparison to the applied magnetic field. Under these assumptions the governing equations of the problem are as below:

CONTINUITY EQUATION:

$$\frac{\partial u}{\partial x} + \frac{\partial v}{\partial y} = 0 \tag{1}$$

MOMENTUM EQUATION:

$$u\frac{\partial u}{\partial x} + v\frac{\partial v}{\partial y} = -\frac{1}{\rho}\frac{\partial p}{\partial x} + \frac{\partial}{\partial y}\left(\upsilon\frac{\partial u}{\partial y}\right) + \frac{\kappa}{\rho}\left(\frac{\partial N}{\partial y} + \frac{\partial^2 u}{\partial y^2}\right) \pm g\beta(T - T_\infty) - \frac{\sigma}{\rho}B^2 u \tag{2}$$

ANGULAR MOMENTUM EQUATION:

$$\rho j\left(u\frac{\partial N}{\partial x} + v\frac{\partial N}{\partial y}\right) = \gamma\frac{\partial^2 N}{\partial y^2} - \kappa\left(2N + \frac{\partial u}{\partial y}\right) \tag{3}$$

ENERGY EQUATION:

$$\rho c_p\left(u\frac{\partial T}{\partial x} + v\frac{\partial T}{\partial y}\right) = \frac{\partial}{\partial y}\left(\lambda\frac{\partial T}{\partial y}\right) + (\mu + \kappa)\left(\frac{\partial u}{\partial y}\right)^2 \tag{4}$$

Where u, v are velocity components in the directions of x and y along and perpendicular to the surface respectively. N is the component of micro -rotation vector normal to the xy -plane, ρ is the density, κ is the vortex viscosity, g is the acceleration due to gravity, β is the coefficient of thermal expansion, γ is the

spin gradient viscosity , j is the micro-inertia density , p is the pressure of the fluid , T is the temperature , υ and λ are the viscosity and thermal conductivity respectively which are the functions of x and y . c_p is the specific heat capacity at constant pressure of the fluid , B is the magnetic intensity and σ is the electrical conductivity . The term $\pm g\beta(T - T_\infty)$ of equation (2) indicates the buoyancy force, where "+" sign refers buoyancy assisting and "-''sign corresponds to the buoyancy opposing the flow regions.

The boundary conditions for the problem are:

$$\left.\begin{aligned} &u(x,0) = bx, \quad v(x,0) = 0, \quad N(x,0) = 0, \quad T(x,0) = T_\infty \\ &u(x,\infty) = U = ax, \quad N(x,\infty) = 0, \quad T(x,\infty) = T_\infty \end{aligned}\right\} \tag{5}$$

Where b < 0 for the shrinking sheet, T_w is temperature on the surface, T_∞ is temperature of the fluid at infinity and U is the free stream velocity of the fluid.

Following Lai and Kulacki [17] let us assume that,

$$\left.\begin{aligned} &\frac{1}{\mu} = \frac{1}{\mu_\infty}[1 + \delta(T - T_\infty)] \text{ or } \frac{1}{\mu} = \Delta(T - T_r) \text{ where } \Delta = \frac{\delta}{\mu_\infty} \text{ and } T_r = T_\infty - \frac{1}{\delta} \\ &\frac{1}{\lambda} = \frac{1}{\lambda_\infty}[1 + \xi(T - T_\infty)] \text{ or } \frac{1}{\lambda} = \varepsilon(T - T_c) \text{ where } \varepsilon = \frac{\xi}{\lambda_\infty} \text{ and } T_c = T_\infty - \frac{1}{\xi} \end{aligned}\right\} \tag{6}$$

where μ_∞ is the viscosity at infinity, Δ and T_∞ are constants , T_r is transformed reference temperature , δ is a constant based on thermal property of the fluid and $\Delta < 0$ for gas , $\Delta > 0$ for liquid. Similarly, ε and T_c are constants and their values depend on the reference state and thermal properties of the fluid i.e., ξ.

To solve equations (1) - (4) subject to the boundary conditions given in equation (5) we use the following similarity transformations,

$$\left.\begin{aligned} &\eta = \left(\frac{a}{\upsilon_\infty}\right)^{\frac{1}{2}} y, \quad p(x,\infty) = p_0 - \frac{\rho a^2}{2}(x^2 + y^2), \quad u(x,y) = axf'(\eta), \\ &v(x,y) = -(a\upsilon_\infty)^{\frac{1}{2}} f(\eta), \quad N(x,y) = -a\left(\frac{a}{\upsilon_\infty}\right)^{\frac{1}{2}} xg(\eta), \quad \theta(\eta) = \frac{T - T_\infty}{T_{w-}T_\infty} \end{aligned}\right\} \tag{7}$$

Where η is the similarity parameter, p_0 is the stagnation pressure. Also from equations (6) and (7), we have,

$$\upsilon = -\upsilon_\infty \frac{\theta_r}{\theta - \theta_r}, \qquad \lambda = -\lambda_\infty \frac{\theta_c}{\theta - \theta_c} \tag{8}$$

Equation of continuity in equation (1) is identically satisfied using equation (6) and therefore the velocity field is compatible with continuity equation and represents the possible fluid motion. Using equations (7) and (8) in equations (2)-(4) we get the following differential equations:

$$(f')^2 - ff'' = 1 + \frac{\theta_r}{(\theta_r - \theta)^2}\theta' f'' + \frac{\theta_r}{\theta_r - \theta} f''' + K(f''' - g') + R\theta - M^2 f' \tag{9}$$

$$fg - g'f = Cg'' + AK(f'' - 2g) \tag{10}$$

$$\frac{\theta_c}{(\theta_c - \theta)^2}(\theta')^2 + \frac{\theta_c}{\theta_c - \theta}\theta'' + P_r f\theta' + P_r E_c\left(\frac{\theta_r}{\theta_r - \theta} + K\right)(f'')^2 = 0 \tag{11}$$

Where

$K = \frac{\kappa}{\mu_\infty}$ is the coupling constant parameter , $C = \frac{\gamma}{\mu_\infty j}$ is the spin gradient viscosity parameter,

$\Pr = \frac{\rho c_p \upsilon_\infty}{\lambda_\infty}$ is the Prandtl number, $M^2 = \frac{\sigma B^2}{\rho a}$ is the magnetic parameter,

$R = \pm \frac{G_{r_x}}{R_{e_x}^2}$ ('+' in assisting flow and '-' in opposing flow) is the buoyancy parameter ,

$E_c = \frac{a^2 x^2}{C_p(T_w - T_\infty)}$ is the Eckert number and $A = \frac{\mu_\infty}{\rho ja}$ is the micro inertia density parameter

Here $Gr_x = \frac{g\beta(T_w - T_\infty)x^3}{\upsilon_\infty x^2}$ is the local Grashoff number and $\mathrm{Re}_x = \frac{Ux}{\upsilon_\infty}$ is the local Reynolds number.

θ_r and θ_c are the dimensionless parameters characterizing the influence of viscosity and thermal conductivity respectively, can be written as:

$$\left.\begin{aligned} \theta_r &= \frac{T_r - T_\infty}{T_w - T_\infty} = -\frac{1}{\delta(T_w - T_\infty)} \\ \theta_c &= \frac{T_c - T_\infty}{T_w - T_\infty} = -\frac{1}{\xi(T_w - T_\infty)} \end{aligned}\right\} \tag{12}$$

The transformed boundary conditions are,

$$\left.\begin{aligned} &f(\eta) = 0, \quad f'(\eta) = b/a = \alpha, \quad g(\eta) = 0, \quad \theta(\eta) = 1 \quad \text{at} \quad \eta = 0 \\ &f'(\eta) = 1, \quad g(\eta) = 0, \quad \theta(\eta) = 0 \quad \text{as} \quad \eta \to 0 \end{aligned}\right\} \tag{13}$$

Here the case $\alpha = 0$ stands for Hiemenz flow towards a solid plate and the case $\propto > 0$ is for the stagnation point over a stretching sheet. In our case of stagnation flow towards a shrinking sheet, hence we take $\propto < 0$.

The two important physical quantities of our interest in the problem are skin friction coefficient (c_f) and Nusselt number (Nu) which are defined as,

$c_f = \frac{2\tau_w}{\rho U_0^2}$, where τ_w, the shear stress at the surface is given by, $\tau_w = \left[(\mu + \kappa) \frac{\partial u}{\partial y} + \kappa N \right]_{y=0}$

And $Nu = \frac{x q_w}{\lambda_\infty (T_w - T_\infty)}$, where q_w, the heat flux is given by , $q_w = -\lambda \left[\frac{\partial T}{\partial y} \right]_{y=0}$

Therefore,

$$c_f \, \mathrm{Re}_x^{1/2} = 2 \left(\frac{\theta_r}{\theta_r - 1} + K \right) f''(0) \tag{14}$$

$$Nu \, \mathrm{Re}_x^{-1/2} = \frac{\theta_c}{\theta_c - 1} \theta'(0) \tag{15}$$

III. Results and Discussion:

The system of differential equations (9 - 11) together with the boundary conditions (13) is solved numerically by using the fourth order of Runge-Kutta integration accompanied with the shooting iteration scheme. The purpose of this study is to bring out the effects of the variable viscosity and variable thermal conductivity on the governing flow with the combinations of the other flow parameters.

The numerical computations have been carried out for various values of magnetic parameter (*M*), Prandtl number (Pr), Eckert number (E_c), buoyancy parameter (R), coupling constant parameter (K), the variable viscosity parameter (θ_r), variable thermal conductivity parameter (θ_c) and micro inertia density parameter (A). In order to illustrate the results graphically, the numerical values of dimensionless velocity distribution $f'(\eta)$, dimensionless micro-rotation distribution $g(\eta)$ and temperature distribution $\theta(\eta)$ with variation of different parameters have been plotted in Figures 1 – 12.

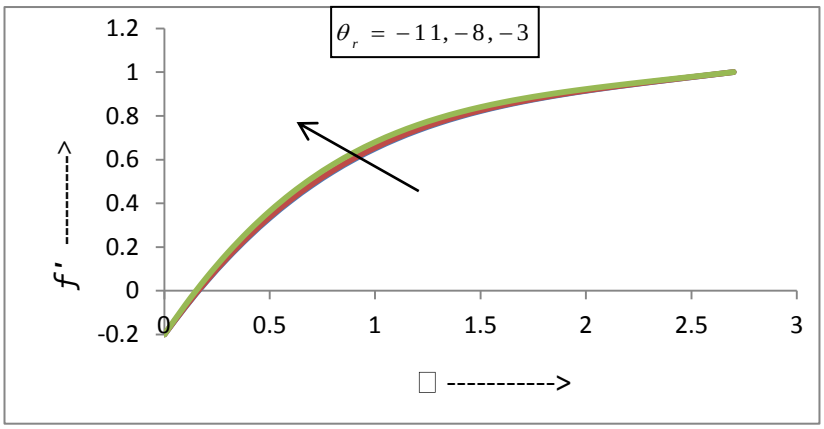

Figure 1. Variation of $f'(\eta)$ for different values of θ_r

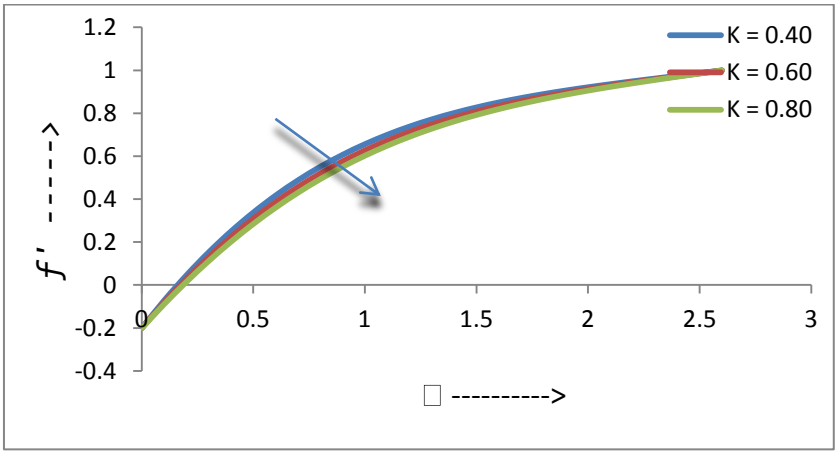

Figure 2. Variation of $f'(\eta)$ for different values of K

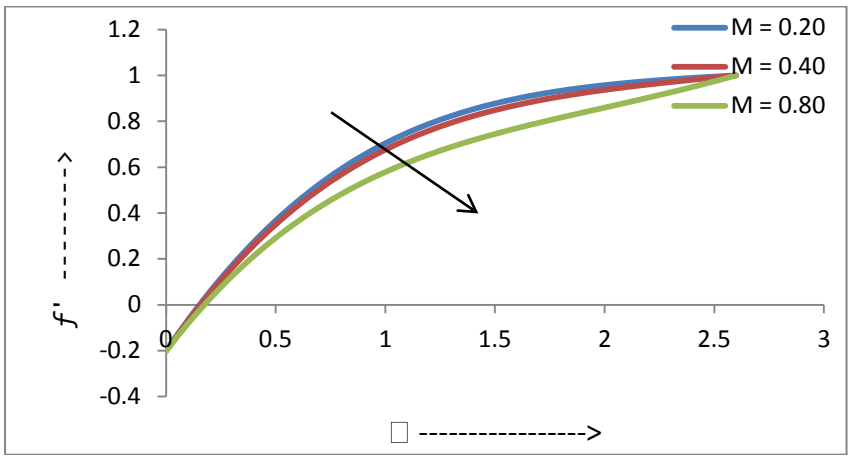

Figure 3. Variation of $f'(\eta)$ for different values of M

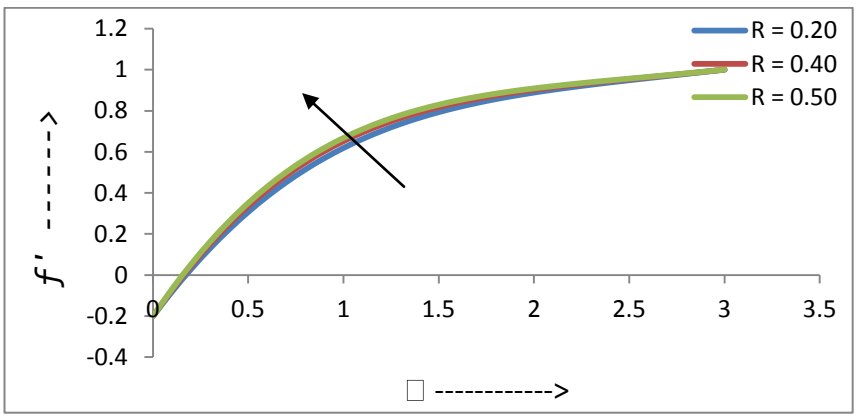

Figure 4. Variation of $f'(\eta)$ for different values of R

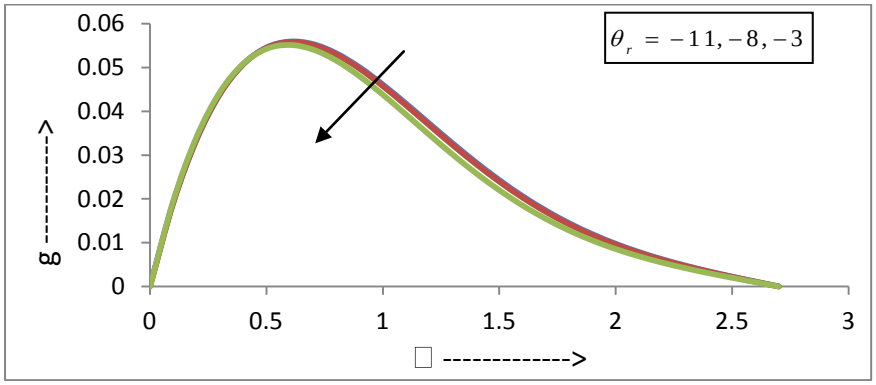

Figure 5. Variation of $g(\eta)$ for different values of θ_r

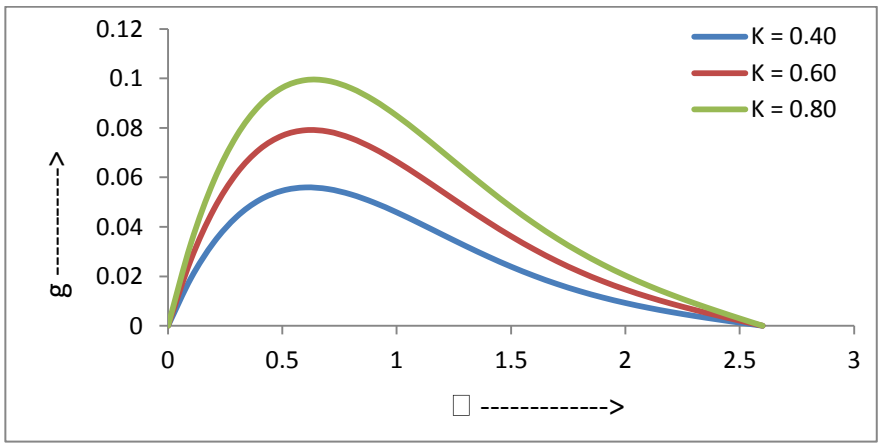

Figure 6. Variation of $g(\eta)$ for different values of K

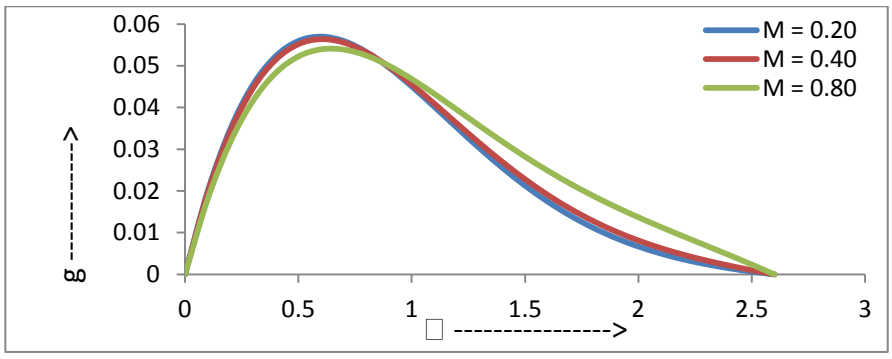

Figure 7. Variation of $g(\eta)$ for different values of M

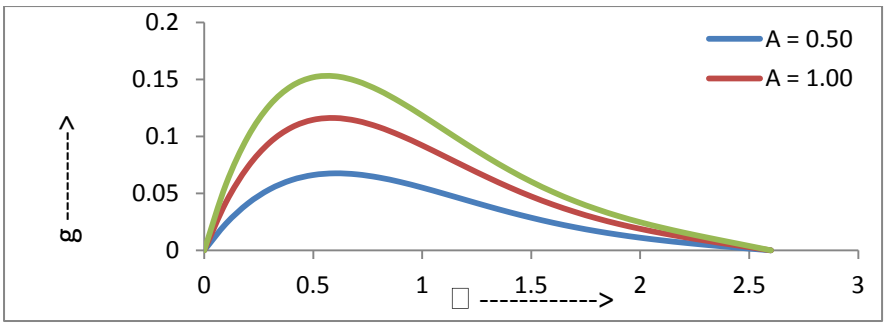

Figure 8. Variation of $g(\eta)$ for different values of A

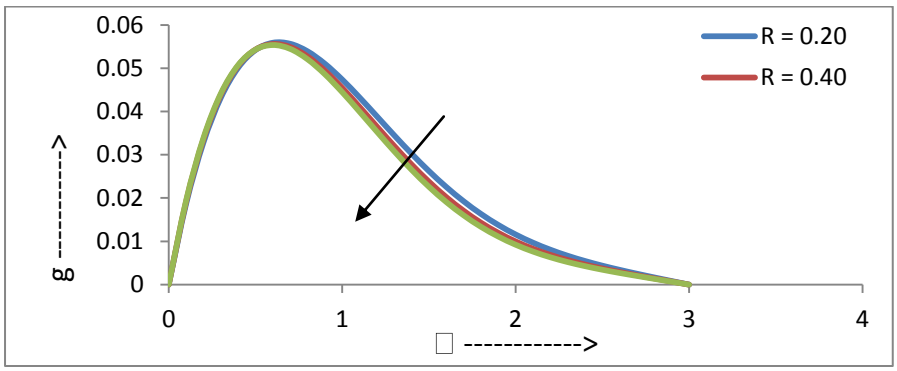

Figure 9. Variation of $g(\eta)$ for different values of R

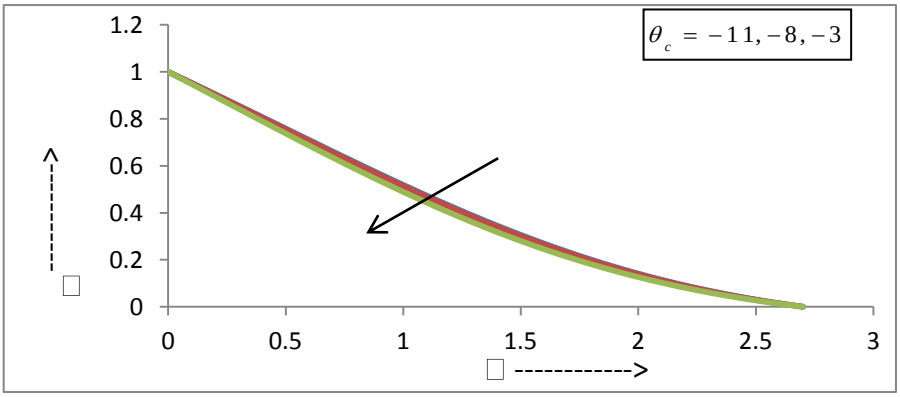

Figure 10. Variation of $\theta(\eta)$ for different values of θ_c

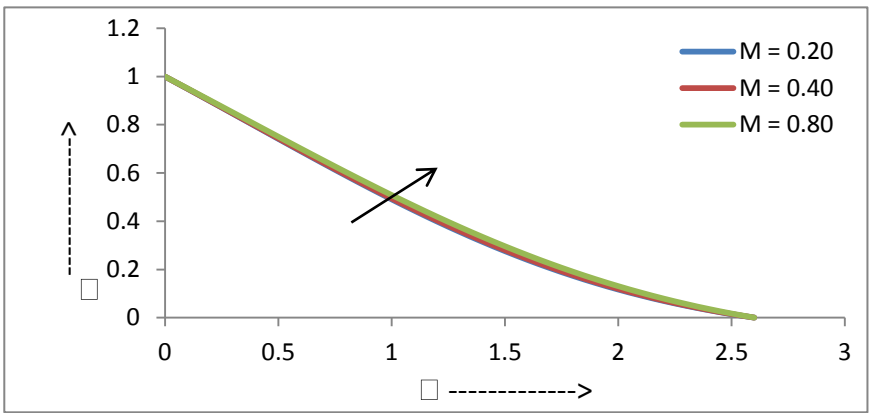

Figure 11. Variation of $\theta(\eta)$ for different values of M

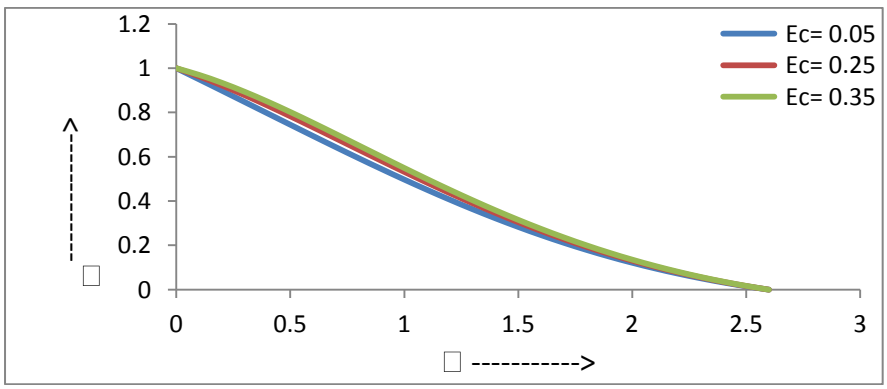

Figure 12. Variation of $\theta(\eta)$ for different values of E_c

The Figures 1- 4 represent the velocity distribution with the variation of viscosity parameter θ_r .coupling constant parameter K , magnetic parameter M , Buoyancy parameter R respectively. It is seen that velocity increases with the increasing values of θ_r and R where as it decreases with the increasing values of M and K . It has been observed that with the variations of thermal conductivity parameter θ_c , micro-inertia density parameter A , Eckert number E_c and Prandtl number Pr the variation of velocity is not significant.

Figures 5 – 9 represents the variation in micro-rotation distribution with the variation of viscosity parameter θ_r , coupling constant parameter K , magnetic parameter M , micro-inertia density parameter A and Buoyancy parameter R respectively. It is observed that micro-rotation decreases with the increasing values of θ_r and R respectively. It is evident from the Figures 6, 7 and 8, the micro-rotation distribution increases with the increasing values of K , M and A respectively. In this case also variation of micro-rotation is not so much significant with the variations of thermal conductivity parameter θ_c , Eckert number E_c and Prandtl number $\Pr$. The Figures (10-12) represents variation of temperature distribution with the variation of thermal conductivity parameter θ_c , Magnetic parameter M and Eckert number E_c . It is observed that temperature decreases as θ_c increases whereas it increases with the increasing values of M and E_c . In several practical applications, the surface characteristics such as friction factor and Nusselt number play important roles and hence, the missing values of $f''(0)$, $g'(0)$ and $\theta'(0)$ for various values of θ_r , θ_c , M , $\Pr$, K and E_c have been derived in Table 1.

Table- 1.

θ_r	θ_c	M	$\Pr$	K	E_c	$\alpha = -0.20$ $R = 0.40$ $C = 1.00$ $A = 0.40$		
						$f''(0)$	$g'(0)$	$\theta'(0)$
- 9	- 5	0.40	0.71	0.40	0.05	1.35553	0.106175	- 0.496973
- 7						1.371888	0.106582	- 0.498339
- 5						1.400093	0.107281	- 0.50069
- 8	**- 9**	0.40	0.71	0.40	0.05	1.364403	0.106458	- 0.478009
	- 6					1.363355	0.106393	- 0.490354
	- 5					1.362749	0.106355	- 0.497576
- 8	- 5	**0.40**	0.71	0.40	0.05	1.362749	0.106355	- 0.497576
		0.80				1.245599	0.098189	- 0.484796
		1.20				1.111045	0.087574	- 0.466789
- 8	- 5	**0.25**	**0.71**	0.40	0.05	1.390798	0.10821	- 0.500322
			1.71			1.375764	0.107211	- 0.589739
			2.21			1.370622	0.10688	- 0.619417
- 8	- 5	0.25	0.71	**0.40**	0.05	1.390798	0.10821	- 0.500322
				0.60		1.284479	0.153271	- 0.489207
				0.70		1.238793	0.173933	- 0.484205
- 8	- 5	0.25	0.71	0.40	**0.02**	1.389789	0.108154	- 0.525639
					0.05	1.390798	0.10821	- 0.500322
					0.08	1.391807	0.108266	- 0.474946

From the Table-1, it is observed that with the increasing values of θ_r and E_c, the values of $f''(0)$ and $g'(0)$ are increasing and the values of $\theta'(0)$ are decreasing for the increasing values of θ_r when all other parameters are fixed. It is seen that with the increasing values of θ_c and $\Pr$, the values of $f''(0)$, $g'(0)$ and $\theta'(0)$ are decreasing. It is also indicated that when the magnetic parameter M and coupling constant parameter K increases, the values of $\theta'(0)$ increases but the reversal trend is observed for $f''(0)$ and $g'(0)$.

IV Conclusions

In this study , the effects of temperature dependent viscosity and thermal conductivity in a mixed convection boundary layer flow of a micropolar fluid towards a heated shrinking sheet in presence of magnetic field is examined. Numerical solutions are presented for the fluid flow and heat transfer characteristics for different values of parameters involved in the problem. The effects of temperature dependent viscosity and thermal conductivity on velocity, micro-rotation and temperature distribution are quite significant. Thus, the present study will serve as a scientific tool for understanding more complex flow problems concerning with the various physical parameters.

References

[1] Eringen ,A.C.,J. Math.Mech.,Vol.16,pp.1

[2] Rashidi, M.M., Erfani, E., A new analytical study of MHD stagnation point flow in pouras media with heat transfer *Computers and Fluids*, 40 , 1, pp. 172-178, 2011.

[3] Hiemenz, K., Die Grenzschicht an einem in den gleichformigen Flussigkeitsstrom eingetauchten geraden Kreiszylinder , Weber, Berlin,Germany,1911

[4] Chamkha, A.J., Issa, C., Effects of heat generation/absorption and thermophoresis on hydromagnetic flow with heat and mass transfer over a flat surface , *International journal of Numerical Methods for Heat and Fluid Flow, 10 (2000), 4, pp. 432-449*

[5] Mahapatra, T.R, Gupta, A.S., Magnetohydrodynamic stagnation-point flow towards a stretching sheet , Acta Mechanica,152, 1-4, pp.191-196, 2001.

[6] Nazar, R., Amin, N., Filip, D., Pop, I., Unsteady boundary layer flow in the region of the stagnation point on a stretching sheet. *International journal of Engineering Science*, 42, 11-12, pp. 1241-1253, 2004.

[7] Abdelkhalek, M.M., The skin friction in the MHD mixed convection stagnation point with mass transfer , International Communications in Heat and Mass Transfer , 33, 2, pp.249-258, 2006.

[8] Yian, L.Y., Amin, N., I., Mixed convection flow near a stagnation point towards a stretching Vertical plate. International journal of heat and mass transfer , 50 , 23-24,pp.4855-4863, 2007.

[9] Sharma, P.R., Singh, G., Effects of variable thermal conductivity and heat source /sink on MHD flow near a stagnation point on a linearly stretching sheet , Journal of Applied Fluid Mechanics, 21, pp.13-21, 2009.

[10] ChenCh.H. ,effect of viscous dissipation on heat on heat transfer in a non-Newtonian liquid film over an unsteady stretching sheet , J.Non-Newton .Fluid ,vol.135(2-3) , pp.128-135, 2006.

[11] Ishak A , Nazar R., Pop I., Heat transfer over a stretching surface with variable heat flux in micropolar fluids , Physics letter A , Vol.372 , pp.559-561, 2008.

[12] Mahanta P.K., Hazarika G.C., Effects of radiation of flow of second grade fluid over a stretching sheet through porous medium with temperature dependent viscosity and thermal conductivity , Int.J.Comp.En.Res.(IJCER),vol.2, ISSN 2250-3005, Dec.2012.

[13] Nazar , R., Amin, N., Filip, D., Pop ,I., Stagnation point flow of a micropolar fluid towards a stretching sheet , Int. J. Of Non-Linear Mechanics, 39(7), pp.1227-1235, 2004.

[14] Chang , C.L., Numerical solution of micropolar fluid flow along a flat plate with wall conduction and boundary effects, Journal of physics D : Applied physics , 396, pp.1132-1140, 2006.

[15] Ishak , A., Nazar, R., Pop, I., MHD flow of a microplar fluid towards a stagnation point on a vertical surface , Computers & Mathematics with Applications, 56, 12, pp.3188-3194, 2008.

[16] RASHIDI .M.M., ASHRAF.M., ROSTAMI.B., RASTEGARI. T., BASHIR.S.,Mixed convection Boundary layer flow towards a heated shrinking sheet by homotopy analysis method, Thermal science,2013 online-First (00):96-96,doi :10,2298/TSCI 130212096R.

[17] Lai F.C. and Kulacki F.A., The effect of variable viscosity and mass transfer along a vertical surface in saturated porous medium, Int.J . Heat and Mass transfer , vol.33 , pp.1028-1031.

ISSN (e): 2250 – 3005 || Volume, 05 || Issue, 07 || July – 2015 ||
International Journal of Computational Engineering Research (IJCER)

A Study to Draw the Relationship between Selected Body Composition Variables and Free Style Swimming Performance of School Boys.

*Dr. Saikot Chatterjee. **Mr. Deb Biswas *** Dr. Bhashkar Chakraborty
** Asst. Prof. Department of Physical Education, University of Kalyani. Nadia, West Bengal, India.*
*** Student M.P.Ed. 2nd Sem. University of Kalyani, Nadia, West Bengal, India. Asst. Teacher Bansberia High School*

ABSTRACT

Swimming emerged as a competitive sport in the 1830s in England. In 1828, the first indoor swimming pool, St George's Baths was opened to the public."" By 1837, the National Swimming Society was holding regular swimming competitions in six artificial swimming pools, built around London. The sport grew in popularity and by 1880, when the first national governing body, the Amateur Swimming Association, was formed, there were already over 300 regional clubs in operation across the country. Weight and body composition are touchy subjects around most pool decks. Though many swimmers try to lose weight (or are told to do so), others believe that extra adipose may help swimming via added flotation as per Archimedes Principle. Others feel that a more curved body shape rounded by fatty tissue may also improve hydrodynamics. Yet despite any flotation benefits, frontal drag may be impaired by excess body mass. In a mixed-gender study, Geladas (2005) studied 263 swimmers aged 12-14 and examined predictors of 100m freestyle performance. In neither gender was body composition or weight significantly correlated with 100m. Several research studies have been conducted to analyze the impact of body or somatotype on sport also numerous studies conducted to assess the effects of body composition on various sporting events but according to the literature available very few studies have been conducted to locate the relationship between bodily fat mass, lean mass, fat percentage with swimming performance etc. thus the author felt encouraged to conduct the study entitled "A Study to Draw the Relationship between Selected Body Composition Variables and Free Style Swimming Performance of School Boys". The researcher conducted a study with 31students aged 13 to 17 years of Hooghly District School Swimming Competition – 2014. From statistical analysis i.e. correlation studies it appears that no positive correlation exists between BF% fat mass and lean mass with 50 mts. freestyle swimming performance.

Key words: *Freestyle swimming, Fat Mass, Body Fat percentage.*

I. INTRODUCTION

According to history 10,000-year-old rock paintings of people swimming were found in the Cave of Swimming near Wadi Sura in southwestern Egypt. An Egyptian clay seal dated between 9000 BCE and 4000 BCE shows four people who are believed to be swimming a variant of the front crawl. More references to swimming are found in the Babylonian has- reliefs and Assyrian wall drawings, depicting a variant of the breaststroke. The most famous drawings were found in the Kebir desert and are estimated to be from around 4000 BCE. The Nagoda bas-relief also shows swimmers inside of men dating back from 3000 BCE. The Indian palace Mohenjo Daro from 2800 BCE contains a swimming pool sized 30m by 60m. An Early modern era Leonardo da Vinci made early sketches of lifebelts. In 1539, Nikolaus Wynmann, a German professor of languages, wrote the first swimming book *Colymbetes.* His purpose was to reduce the dangers of drowning.

The Olympic Games were held in 1896 in Athens, a male-only competition. Six events were planned for the swimming competition, but only four events were actually contested: 100 m, 500 m, and 1200 m freestyle and 100 m for sailors. The first gold medal was won by Alfred Hajos of Hungary in the 100m freestyle. Hajos was also victorious in the 1200m event, and was unable to compete in the 500 m, which was won by Austrian Paul Neumann.

The swimming training is tried by using hydrodynamics technology. We research the optimization of swimming from analyzation of waves made by swimmer.

There are many reasons why people swim, from swimming as a recreational pursuit to swimming as a necessary part of a job or other activity. Swimming may also be used to rehabilitate injuries, especially various cardiovascular injuries and muscle injuries.

Swimming emerged as a competitive sport in the 1830s in England. In 1828, the first indoor swimming pool, St George's Baths was opened to the public."" By 1837, the National Swimming Society was holding regular swimming competitions in six artificial swimming pools, built around London. The sport grew in popularity and by 1880, when the first national governing body, the Amateur Swimming Association, was formed, there were already over 300 regional clubs in operation across the country.

Several research studies have been conducted to analyze the impact of body or somatotype on sport also numerous studies conducted to assess the effects of body composition on various sporting events but according to the literature available very few studies have been conducted to locate the relationship between bodily fat mass, lean mass, fat percentage with swimming performance etc. thus the author felt encouraged to conduct the study entitled "A STUDY TO DRAW THE RELATIONSHIP BETWEEN SELECTED BODY COMPOSITION VARIABLES AND FREE STYLE SWIMMING PERFORMANCE OF SCHOOL BOYS".

PURPOSE OF THE STUDY:

The purposes of the study are as follows:

(i) The study was formulated to explore the relationship between Fat mass and 50 mts. swimming performance.

(ii) The study was formulated to explore the relationship between Body Fat % and 50 mts.
swimming performance.

METHODOLOGY: The researcher randomly selected 31 boys within the age group 13 to 17 years from Hooghly District School Swimming Competition – 2014 as the volunteers of his study. The criterion measures are as follows: As Personal Data – Age, Height, Weight and lean mass, fat mass and body Fat percentage were estimated as measures of body composition.

Age: The age of the subjects were noted from order of events record of each subject.

Height- Each subject was asked to stand erect on a horizontal surface and stretch as much as possible taken in case that heels are touching in front of on wall. The highest point head touching the wall was recorded in (cm).

Weight- The subject stood on the standard weighting machine maintains erect posture. The body weight was recorded in (kg).

For estimation of Lean Mass Fat Mass and Body Fat percentage, in case of 13 – 17 Age boy's. Five skin measurements were like - Abdominal, Chest, Thigh, Suprailiac, & Triceps were measured.

RESULT AND DISCUSSION

In this part of the research report tables depicting descriptive statistics inferential statistics and related discussion have been presented.

Descriptive statistics of personal data is as follows:

Table-1 Mean and SD of age height and weight of the swimmers

	Mean	SD
Age yrs.	14	00
Height cms.	162.26	5.71
Weight kgs.	50.26	7.95

According to table no. 1 the mean age of the swimmers is 14 years. The mean height is 162.26 and their SD is 5.71. The mean weight is 50.26 and SD is 7.95 respectively.

Table-2 Pearson Correlation between BF% fat mass and lean mass.

Correlations

		BF%	BF	Lean Mass	Time secs
BF%	Pearson Correlation	1	.963**	.512	.257
	Sig. (2-tailed)		.000	.051	.355
	N	15	15	15	15
BF	Pearson Correlation	.963**	1	.705**	.255
	Sig. (2-tailed)	.000		.003	.359
	N	15	15	15	15
Lean Mass	Pearson Correlation	.512	.705**	1	.239
	Sig. (2-tailed)	.051	.003		.391
	N	15	15	15	15
Time secs	Pearson Correlation	.257	.255	.239	1
	Sig. (2-tailed)	.355	.359	.391	
	N	15	15	15	15

**. Correlation is significant at the 0.01 level (2-tailed).

The above table shows Pearsons correlation (product moment method) between 50 mts. freestyle swimming performance and the variables BF %, Fat Mass and Lean Mass. From the data analysis it appears that no positive correlation exists between BF%, fat mass and lean mass with 50 mts. freestyle swimming performance.

Table-3 Correlation between BF% fat mass and lean mass. (Non-Parametric)

Correlations

			BF%	BF	Lean Mass	Time secs
Kendall's tau_b	BF%	Correlation Coefficient	1.000	.907**	.517**	.301
		Sig. (2-tailed)	.	.000	.008	.123
		N	15	15	15	15
	BF	Correlation Coefficient	.907**	1.000	.615**	.364
		Sig. (2-tailed)	.000	.	.001	.060
		N	15	15	15	15
	Lean Mass	Correlation Coefficient	.517**	.615**	1.000	.096
		Sig. (2-tailed)	.008	.001	.	.620
		N	15	15	15	15
	Time secs	Correlation Coefficient	.301	.364	.096	1.000
		Sig. (2-tailed)	.123	.060	.620	.
		N	15	15	15	15
Spearman's rho	BF%	Correlation Coefficient	1.000	.964**	.648**	.361
		Sig. (2-tailed)	.	.000	.009	.187
		N	15	15	15	15
	BF	Correlation Coefficient	.964**	1.000	.782**	.368
		Sig. (2-tailed)	.000	.	.001	.177
		N	15	15	15	15
	Lean Mass	Correlation Coefficient	.648**	.782**	1.000	.164
		Sig. (2-tailed)	.009	.001	.	.558
		N	15	15	15	15
	Time secs	Correlation Coefficient	.361	.368	.164	1.000
		Sig. (2-tailed)	.187	.177	.558	.
		N	15	15	15	15

**. Correlation is significant at the 0.01 level (2-tailed).

Since the number of subjects was less both parametric and non-parametric correlations were computed to assess the degree of relationship between the 50 mts. freestyle swimming performance and the variables BF %, Fat Mass and Lean Mass.

From the correlation studies it appears that no positive correlation exists between BF% fat mass and lean mass with 50 mts. freestyle swimming performance.

Lätt (2009) tracked 26 female swimmers for two years and examined relationships between biomechanical, bioenergetic, and anthropometric factors. Anthropometric factors included body mass, body fat percentage, fat free mass, bone mineral mass, and total bone density (authors also tracked age, height, and arm span). At the two year follow up, biomechanical factors were most predictive of performance, followed by bioenergetics. Anthropometrics had the weakest relation to performance compared to other factors.

In a mixed-gender study, Geladas (2005) studied 263 swimmers aged 12-14 and examined predictors of 100m freestyle performance. For boys, upper extremity length, horizontal jump, and grip strength were significant predictors of 100 m freestyle performance. In girls, body height, upper extremity and hand length, shoulder flexibility, and horizontal jump were all significantly related to 100 m freestyle time. In neither gender was body composition or weight significantly correlated with 100m performance. Juriimae (2007) later found similar results among 29 young boys in a 400m time trial, as stroke mechanics, arm length, and in-water VO2 peak were most correlated with performance while body weight and body composition showed no significant performance relationship. Some findings of eminent scholars have been presented above and it is somehow clear from the presentation that the results of the presentation have close association with those above findings.

Findings: From the correlation studies it appears that no positive correlation exists between BF% fat mass and lean mass with 50 mts. freestyle swimming performance.

Conclusion: Thus the researcher arrives at the specific conclusion that the body composition variables like BF%, Fat Mass and Lean Body Mass does not have any close association with 50Mts. swimming performance of male swimmers. On the other way the perception like greater amount of Body fat is better for swimming performance or Body fat facilitates swimmer with greater bouncy is like a misconception.

References

[1]. Geladas ND, Nassis GP, Pavlicevic S. Somatic and physical traits affecting sprint swimming performance in young swimmers. Int J Sports Med. 2005 Mar;26(2):139-44.

[2]. Zampagni ML, Casino D, Benelli P, Visani A, Marcacci M, De Vito G. Anthropometric and strength variables to predict freestyle performance times in elite master swimmers. J Strength Cond Res. 2008 Jul;22(4):1298-307. doi: 10.1519/JSC.0b013e31816a597b.

[3]. Lätt E, Jürimäe J, Haljaste K, Cicchella A, Purge P, Jürimäe T. Physical development and swimming performance during biological maturation in young female swimmers. Coll Antropol. 2009 Mar;33(1):117-22.

[4]. Poujade B, Hautier CA, Rouard A. Determinants of the energy cost of front-crawl swimming in children. Eur J Appl Physiol. 2002 May;87(1):1-6. Epub 2002 Feb 20.

[5]. Jürimäe J, Haljaste K, Cicchella A, Lätt E, Purge P, Leppik A, Jürimäe T. Analysis of swimming performance from physical, physiological, and biomechanical parameters in young swimmers. Pediatr Exerc Sci. 2007 Feb;19(1):70-81.

.

ISSN (e): 2250 – 3005 || *Volume, 05* || *Issue, 07* || *July – 2015* ||
International Journal of Computational Engineering Research (IJCER)

Performance of Thermal Energy Storage System with Finned Spherical Capsules

T. Siva gowthami, R. Meenakshi reddy
[1]*Department of Mechanical Engg., G.P.R College of Engineering, Andhra Pradesh, India.*
[2]*ASSOCIATE PROFESSOR (Department of mechanical engg,G.P.R college of engineering, Andhra Pradesh, India.)*

ABSTRACT

Due to past depletion of conventional energy sources and ever increasing the demand of energy, many researchers started paying attention to renewable energy sources. Thermal energy storage is one key of technologies for energy conservation and has recently developed to a point where it can have a significant impact on modern technologies. The present work deals with the study of finned spherical capsules, the finned sphere is filled with the stearic acid as phase change material. Water used as the heat transfer fluid.HTF occupying space left between the finned spherical containers in thermal energy storage tank. Simulations of the charging and discharging process are performed and obtained results are compared with the previous theoretical results.

KEYWORDS: *Heat transfer fluid, PCM, Thermal energy storage, Latent heat, Charging process, Discharging process, TES tank.*

I. Introduction

In recent years, due to problem of past depletion of conventional energy sources and increasing the demand of energy, as well as increasing attention towards the usage renewable energy resources, Thermal energy storage is one of the important measures in energy conversion systems. Thermal energy storage is the method to be used in conventional energy resources. In this case thermal energy storage is important to improve thermal energy efficiency. Energy storage is combining with the solar collectors and photo voltaic systems. The thermal energy storage utilized at various industrial purposes. Thermal energy stored in three types. These are sensible heat storage, latent heat storage, thermo chemical cold and heat storage. The thermal energy storage methods most commonly used as sensible heat storage, latent heat storage methods. The sensible heat storage method having disadvantages also i.e. unit volume heat storage capacity is low at storage medium and during charging and discharging process sensible heat storage behaves like a non isothermal. In latent heat storage the small volume storing large amount of energy with the solid liquid phase change has received considerable attention. High storage density and heat charging and discharging process at constant temperature. Latent heat storage system plays an important role in energy conservation of environmental conditions. Latent heat storage having high comparison with the sensible heat storage. In which the material undergoes to phase change due to present of latent heat of fusion. A lot of research work has been carried out on sensible heat storage materials and systems in the past and present technology for their utilization and also well developed. Cool thermal energy storage using by the latent heat storage and it offers good option why because it is having high storage density at constant temperature. The principle of latent heat system is change of state. One of the most popular systems is latent heat storage system. The latent heat system is stored energy in the process of encapsulated phase change material. These are uses cylindrical geometries with fins and without fins, cans, plates or spherical capsules. The method of encapsulation is one of the attractive methods. It seems offers number of advantages.

In spherical capsules on energy storage very limited no of studies are found. Saitosh and hirose (1986) investigated experimental and theoretical of thermal characteristics in phase change thermal energy storage by using spherical capsules. The variation of HTF the inlet and outlet temperature difference, The capsule material, the thermal performance of energy storage unit were studied compared with the experimental results of a prototype LHS unit with the capacity of 300L. A very number of studies are found thermal performance of latent heat storage systems means PCM in various geometries. Siva Gowthami et.al studied the charging and discharging process of a finned spherical LHS capsule with stearic acid as PCM. Her experimental results demonstrated that, compared to charging process and discharging process PCM melts faster and it come to solid state taking long time.

The objective of the present work is to study on the thermal performance of a packed bed latent heat thermal energy storage unit integrated with constant heat source. The packed bed contained spherical capsules these contained with encapsulated PCM. The spherical capsules surrounded by the SHS material. Parametric studies were carried out to examine the effects of porosity and HTF flow rates on the performance of the storage unit for varying inlet fluid temperatures. Discharging is carried out by batch wise processes and both continuous to recover store heat.

II. Experimental investigation and setup

It consists of insulated thermal energy storage tank; PCM encapsulated finned spherical capsules, water heaters, storage tank, flow meter and circulating pump. A photographic view of experimental set up is shown below figure. The 380mm diameter and 500mm height stainless steel TES tank has a capacity of 52L to supply hot water for a family of 4 to 5 persons. The shower plate is provided on the top of the tank is to get uniform flow of HTF. The water tank is kept beside the storage tank.TES tank is supplied by HTF from water tank through pump. Spherical capsule of 70 mm outer diameter and 0.8mm thickness inserted with fins of 0.6mm. Because of these fins temperature will be equilibrium at the middle of the spherical ball. The total number of balls in the storage tank is 92. The spherical balls uniformly packed in five layers each supported by wire mesh. Stearic acid used as PCM with melting temperature of 56±1◦c and water is used as both SHS material and HTF.

A flow meter is having accuracy of ±3% is used to measure the flowrate of HTF. The centrifugal pump is used to circulate the HTF from the top of the storage tank. The TES tank was divided in to four segments along its axial direction, thermo couple wires are placed at the inlet, outlet and four segments of thermal energy storage tank. These are used to measure the inlet and outlet temperature of HTF. Another five thermocouple wires are placed at finned spherical capsules to measure the temperature of PCM. The total numbers of thermo couple wires are eleven. These are connected to a temperature indicator. It provides instantaneous digital outputs.

III. Experimental procedure

The water tank connected with the 2200W capacity heaters. The water is heated with the heaters and the temperature rise up to 80◦c. The hot water is circulating in to the storage tank with the help of centrifugal pump. The hot water passes through the finned spherical balls. The finned spherical balls are immersed in hot water. Several experiments are conducted at the different flow rates of HTF. The inlet temperature is varied at different experiments.

During the charging process the HTF is stored in storage tank after some time the hot water is circulated through the TES tank continuously. The heat energy is transfer in to the finned spherical capsules and at the beginning of the charging process the temperature of the PCM in finned spherical capsules is 32◦c.it is very lower to the melting temperature. Initially the heat energy stored inside the finned spherical capsules then it is started to reach the melting temperature. In TES tank energy storage is achieved by melting the PCM at certain temperature. PCM will be super heated at constant temperature this is the charging process. The sensible heat energy stored in the form of liquid PCM. The variations of PCM temperatures and HTF temperatures are recorded with the interval of 3 minutes. The charging process is continued to reach the PCM temperature 80◦c.

In discharging process the experiments carried out in to two methods. First method is continuous process and second one is the batch wise process. In the first method the cold water is continuously circulated in to the storage tank. The cold water temperature is 28◦c.it is recovered to heat energy. The second method is step by step method. First of all 25lit/min water was withdrawn from TES tank and it is mixed with the cold water at 28◦c.Recorded the PCM temperatures at the time interval 10mins, this discharging process is continued until the temperature of PCM reaches 45◦c.

IV. Results and discussions

The temperature variations of PCM and HTF are recorded in thermal energy storage tank for different positions. And the mass flow rates of charging and discharging processes are also recorded. Different mass flow rates are studied in detail.

"4.1.Charging process"

The temperature histories of PCM and HTF are taken in four segments of the thermal energy storage tank. These are taking as X/L=0.25,0.50,0.75and 1. Where X is the axial distance from top of the TES tank and L is the length of the TES. The figure A represents the temperature variation of the heat transfer fluid inside the storage tank with the mass flow rate of 2lit/min and observed the temperature of HTF increases gradually and its temperature reaches 73◦c or 74◦c and then remains nearly constant around 78◦c for a period of 2hrs during which the PCM undergoes to phase changes at 56±1◦c.after that the HTF temperature increases up to 76◦c or 78◦c.

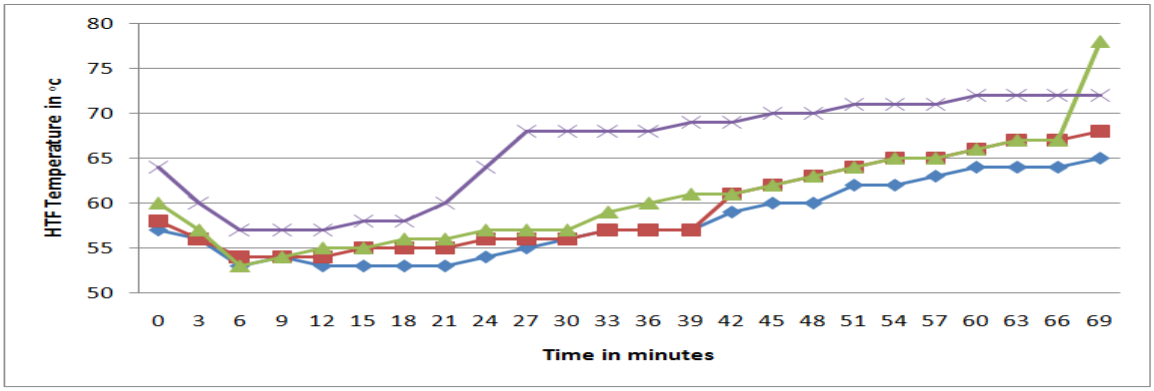

"Figure A.HTF Temperature @ 2 Lit/Min"

Fig B represents the temperature distribution of PCM during the charging process for the mass flow rate of 2lit/min. From the figure it was observed that PCM temperature increased rapidly from 57◦c at which PCM starts melting. During the charging process temperature of all segments reaches up to70◦c. In the above two figures we observed that the inlet temperature and outlet temperatures of TES are equal during the phase change of PCM. Due to this reason the TES tank water temperature increases gradually to the HTF inlet temperature. These are supplied from the hot water tank heated by the heaters. At this stage heat transfer rate from HTF to the PCM is higher than the HTF received from the heaters. Hence it is possible to decreasing the charging time high heating of water.

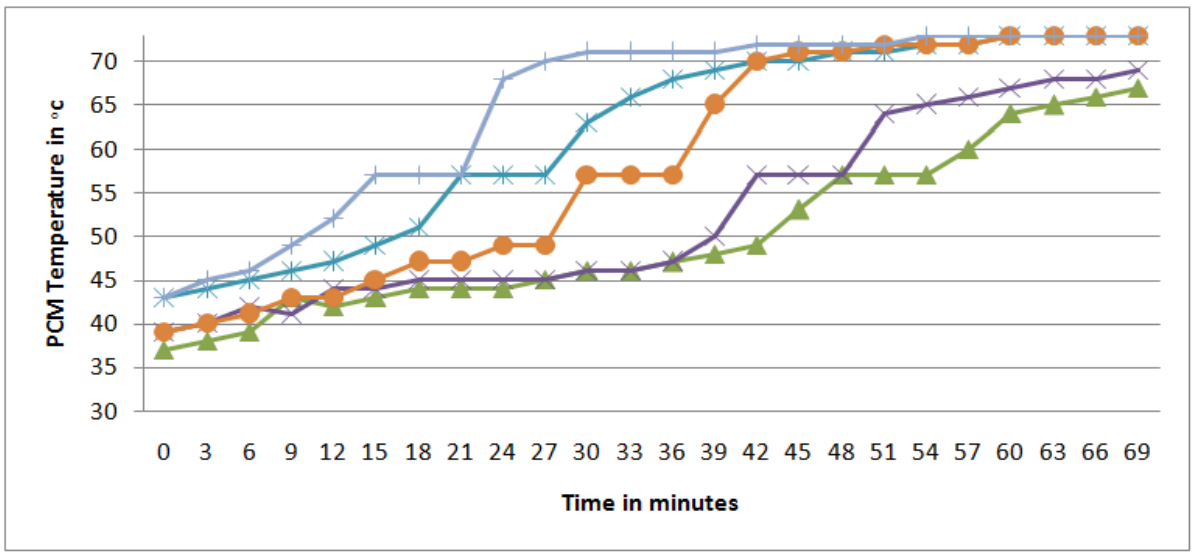

"Figure B.PCM Temperature @ 2 Lit/Min"

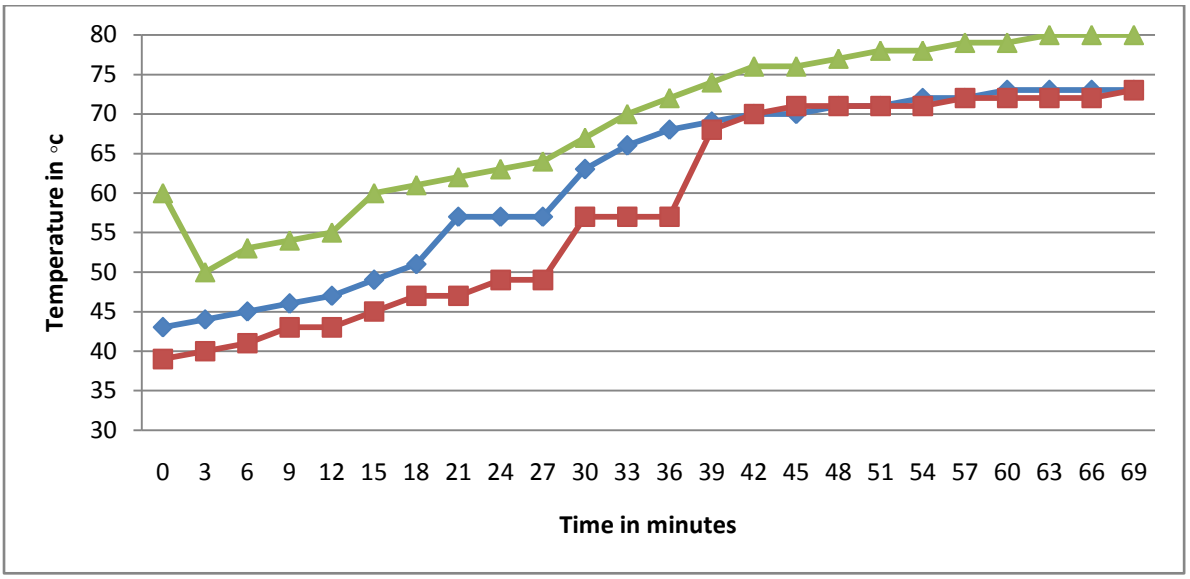

"Figure C. Comparison between PCM & HTF Temperatures"

Fig c shows the comparison of PCM temperature and HTF temperatures at segment 2 of thermal energy storage tank. The instantaneous amount of heat transfer to the PCM depends upon the Heat transfer between the HTF and PCM at a given time. During the charging process PCM absorbs more heat from HTF due to higher resistance offered by solid PCM for heat flow. Fig C illustrates temperature comparison between HTF and PCM after completion of 105 min from the initial process for the case with a mass flow rate of 2lit/min. The temperature of HTF and PCM will be increased and the charging process is continued until the PCM attempts 80◦c.

Fig D illustrates the effect of varying the mass flow rate of HTF (2, 4 lit/min) during the charging process of the storage tank. In the phase transition process of PCM, time required will be less when flow rate increases. The figure shows that charging time decreases when the flow rate increases. This is because an increase in fluid flow rates translates in to an increase in heat transfer coefficient between the HTF and PCM finned spherical capsules.

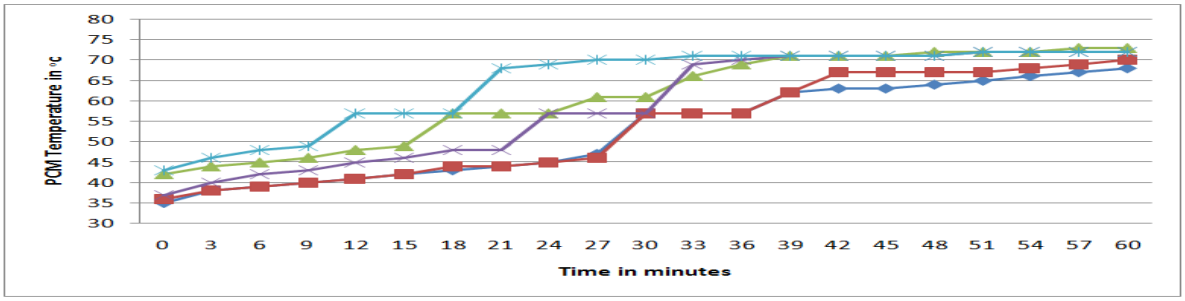

"Figure D. PCM Temperature @ 4 Lit/Min

"4.2.Discharging process"

Fig E represents the temperature distribution of PCM during batch wise in discharging process. It is seen from the figure the temperature drop is large. Until the storage tank losses sensible heat due to mixing of inlet water at a temperature of 32◦c. and observed PCM temperature drop in long duration, as PCM releases its latent heat. During the discharge process the temperature of the finned spherical capsules nearly constant for 25 min and at batch wise process nearly constant temperature occurs over duration of 40 min. The inlet water immediately extracts heat from the storage tank. The temperature decreases after a solidification of PCM. The rate of temperature drop is not high beginning of the discharging process. The temperature difference between the PCM and HTF is low. The solid PCM releases its sensible heat

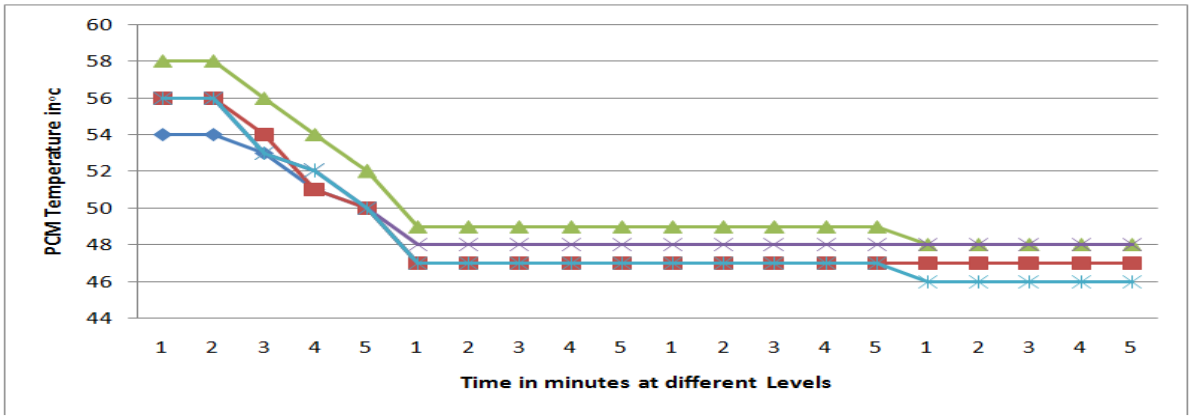

"Figure E. PCM Temperature during discharging"

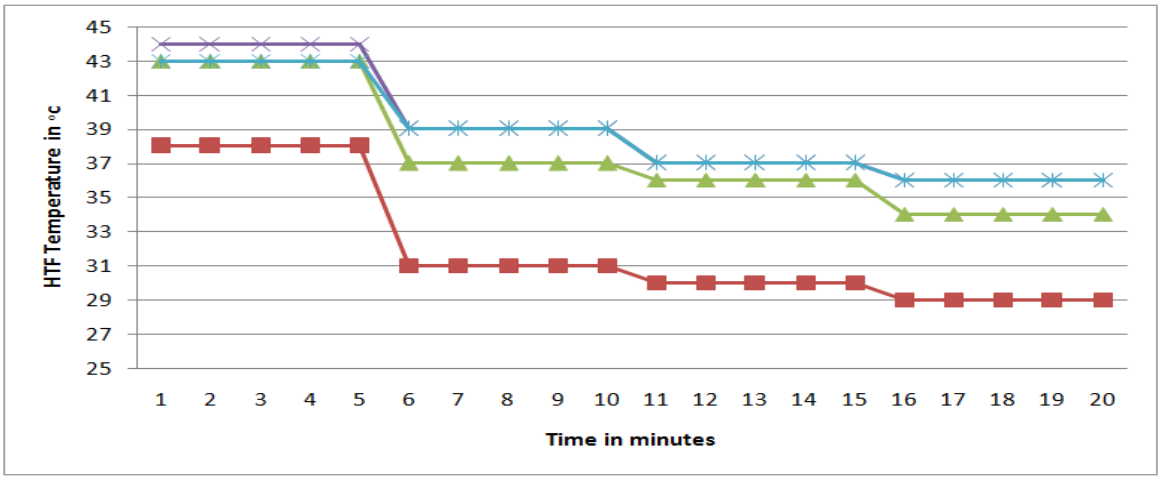

"Figure F. HTF Temperature during discharging"

Figure F. shows temperature distributions of HTF during both continuous and batch wise process. At the beginning of the discharge process the rate of heat recovery is very large. Change in thermal resistance of the solidified layer time is decreased. The temperature difference between HTF and solidifying PCM decreases. The HTF outlet temperature is continuously changes with time. This type of process is not suitable for practical applications

In the case of batch wise process 25L/min hot water is drawn from the storage tank and same quantity of cold water at 32◦c enter in to the storage tank at average temperature of 45◦c.entaire storage tank is filled with the cold water. After completion of the filling the storage tank the temperature of HTF is increases. After a retention period of 10mins the tank increases by gaining heat from finned spherical capsules. The variation of HTF is also shown in the graph.

Five batches of 25L of hot water at an average temperature of 45◦c.these are obtained at 60min time interval. Another batch of hot water at a temperature of 43◦c.it is withdrawn after 40min.the heat extraction from the finned spherical capsules is very slow. As the temperature difference between HTF and PCM is small. At this batch large quantity of water is added the time duration is very high. When considering above model of discharging process of the total system approaches equilibrium temperature nearly 43-45◦c.it is best suited method for the thermal energy storage of finned spherical capsules.

"5.Conclusion"

A thermal energy storage system has been developed for the use of hot water at an average temperature of 45◦c for the domestic applications using combined sensible heat storage and latent heat storage concept. The charging process experiments are conducted at the thermal energy storage unit. These are study its performance by integrating with the constant heat source. The temperature histories of HTF and PCM and energy storage characteristics are studied.

In detailed thermal analysis of solid liquid phase changes are performed. The simulations of the charging mode is performed and results are obtained compared against the previous results. The results are compared temperature distribution of HTF and finned spherical capsules temperature. It is concluded that the mass flow rate has been significant effect on the heat extraction rate from the constant heat source, which in turn affects the rate of charge of thermal energy storage tank. Experiment were conducted for continuous and batch wise discharging process.

References

[1]. N.H.S. TAY ,F. Bruno, M.Belusko , Experimental validation of a CFD model for tubes in a phase change thermal energy storage systems, appl.energy 91(1)(2012)309-319.

[2]. M, Faizal, R.Saidur, S.mekhilef, "Energy, economic and environmental analysis of metal oxides nano fluid for flat-plate collector"ln; presented at the 4th international conference on energy and environment;2013.

[3]. Amrit om Nayak,G.Ramkumar,T.manoj and R.vinod "comparative study between the experimental analysis and CFD software Analysis of PCM material in Thermal Energy Storage System" solar energy1994 ppl143-154.

[4] lippong tan, yuenting kwok,ahbijit date,"numerical analysis of natural convection effects in latent heat storage using different fin shapes "heat transfer 13(1998)297-318

[5] N.A.M. Amin,F. Bruno,M. Belusko "effectiveness-NTU correlation for low temperature PCM encapsulated in spheres",appl.energy(1)(2012)

[6] N.A.Rahim, E.Osterman, v.v tyagi "Review of PCM based cooling technologies for buildings"15(2)(2011)